ANTIOXIDANTS & REDOX SIGNALING
Volume 30, Number 12, 2019

DOI: 10.1089/ars.2017.7375

Discoveries

ORIGINAL RESEARCH COMMUNICATION

Crosstalk Between Connexin32 and Mitochondrial Apoptotic Signaling Pathway Plays a Pivotal Role in Renal Ischemia Reperfusion-Induced Acute Kidney Injury

Chaojin Chen,[1,*] Weifeng Yao,[1,*] Shan Wu,[1] Shaoli Zhou,[1] Mian Ge,[1] Yu Gu,[1] Xiang Li,[1] Guihua Chen,[2] Joseph A. Bellanti,[3] Song Guo Zheng,[4] Dongdong Yuan,[1] and Ziqing Hei[1,5]

Abstract

Aims: Perioperative acute kidney injury (AKI) resulting from renal ischemia reperfusion (IR) is not conducive to the postoperative surgical recovery. Our previous study demonstrated that reactive oxygen species (ROS) transmitted by gap junction (GJ) composed of connexin32 (Cx32) contributed to AKI. However, the precise underlying pathophysiologic mechanisms were largely unknown. This study focuses on the underlying mechanisms related to ROS transmitted by Cx32 responsible for AKI aggravation.

Results: In a set of *in vivo* studies, renal IR was found to cause severe impairment in renal tissues with massive ROS generation, which occurred contemporaneously with activation of NF-κB/p53/p53 upregulated modulator of apoptosis (PUMA)-mediated mitochondrial apoptosis pathways. Cx32 deficiency alleviated renal IR-induced AKI, and simultaneously attenuated ROS generation and distribution in renal tissues, which further inhibited NF-κB/p53/PUMA-mediated mitochondrial apoptotic pathways. Correspondingly, in a set of *in vitro* studies, hypoxia reoxygenation (HR)-induced cellular injury, and cell apoptosis in both human kidney tubular epithelial cells (HK-2s) and rat kidney tubular epithelial cells (NRK52Es) were significantly attenuated by Cx32 inhibitors or Cx32 gene knockdown. More importantly, Cx32 inhibition not only decreased ROS generation and distribution in human or rat kidney tubular epithelial cells but also inhibited its downstream NF-κB/p53/PUMA-mediated mitochondrial apoptotic pathway activation.

Innovation and Conclusion: This is the first identification of the underlying mechanisms of IR-induced renal injury integrally which demonstrates the critical role played by Cx32 in IR-induced AKI. Moreover, GJ composed of Cx32 manipulates ROS generation and distribution between neighboring cells, and alters activation of NF-κB/p53/PUMA-mediated mitochondrial apoptotic pathways. Both inhibiting Cx32 function and scavenging ROS effectively reduce mitochondrial apoptosis and subsequently attenuate AKI, providing effective strategies for kidney protection. *Antioxid. Redox Signal.* 30, 1521–1538.

Keywords: connexin32, renal ischemia reperfusion, acute kidney injury, ROS, mitochondrial apoptosis

Introduction

ACUTE KIDNEY INJURY (AKI) commonly occurs in different kinds of renal surgeries (3, 5, 51), which not only prolongs the length of hospital stay but also severely affects patient survival (27, 29). Reasons for this complication are complex and involve several factors, among which renal hypoperfusion caused by hypotension is considered to be one of the most important independent risk factors (8, 12, 32). Even with major advances in medical care and basic research

[1]Department of Anesthesiology, The Third Affiliated Hospital of Sun Yat-sen University, Guangzhou, People's Republic of China.
[2]Guangdong Provincial Key Laboratory of Liver Disease Research, The Third Affiliated Hospital of Sun Yat-sen University, Guangzhou, People's Republic of China.
[3]Departments of Pediatrics and Microbiology-Immunology, Georgetown University Medical Center, Washington, District of Columbia.
[4]Department of Medicine, Milton S Hershey Medical Center, Penn State University, State College, Pennsylvania.
[5]Department of Anesthesiology, Yuedong Hospital, The Third Affiliated Hospital of Sun Yat-sen University, Meizhou, People's Republic of China.
*These authors contributed equally to this work.

Innovation

This study shows that renal ischemia reperfusion (IR) results in a great deal of reactive oxygen species (ROS) production and NF-κB/p53/PUMA-mediated mitochondrial apoptosis, which could be regulated by connexin32 (Cx32) function. More importantly, Cx32 function inhibition or gene deletion alleviates renal IR-induced damages effectively through regulating the content of ROS and its downstream NF-κB/p53/PUMA-mediated mitochondrial apoptosis. This is the first description of a possible mechanism of Cx32-mediated renal IR injury that may be helpful in the development of novel therapeutic interventions aimed at minimizing renal IR-induced kidney injury.

during the past decades, clinical outcomes of ischemia reperfusion (IR)-induced AKI not only continue to remain poor but also the mechanisms contributing to this complication are still unclear (32, 37). Therefore, there is urgent need to explore the specific mechanisms of AKI and develop effective strategies for renal protection.

Our group first reported that connexin32 (Cx32) might be an important cause of AKI, which could be attenuated by Cx32 inhibition but exacerbated by Cx32 enhancement (22). However, underlying mechanisms were not extensively explored. Thus, this study mainly focuses on the underlying reasons for AKI aggravation caused by Cx32. Connexin is a large family of transmembrane proteins contained in nearly all human organs and tissues.

Until now, about 21 isoforms have been purified and separated. Six connexins compose a hemichannel, two of which are found in neighboring cells docked together forming an integral intercellular channel, called gap junction (GJ), which regulates the direct cell-to-cell signaling transfer of several metabolites such as calcium, trisphosphate, reactive oxygen species (ROS), cyclic adenosine monophosphate, cyclic guanosine monophosphate, and glutathione (15, 35, 54). This type of signaling transfer has stimulated the attention of many researchers, because it is not only essential for many physiological events but also related to the development of various diseases.

ROS is but one of the few signals that can be transmitted through GJ, especially because of its Cx32 content, which regulates ROS generation and distribution in kidneys (22). This view has been verified by our previous studies that showed that posthypoxic ROS production could not only be reduced by propofol, whose protective effects were reinforced by Cx32 inhibition, but also strengthened by Cx32 enhancement (22). However, the mechanism regulating ROS production by Cx32 in kidneys after IR and its importance in causing AKI remain unclear.

ROS is the product of oxygen reduction in the process of aerobic respiration, which is consistently involved in physiologically mediated cell signal transduction and host defense processes. However, excessive ROS generation will cause oxidative stress, redox signaling pathway disruption, and even cell apoptosis (36, 40, 48). We have observed that ROS mediates apoptosis *via* a mitochondria-associated mechanism in renal proximal tubule cells (17, 19, 45). Others have reported that ROS-dependent NF-κB and p53 unregulated modulator of apoptosis (PUMA) pathway activation participates in cell apoptosis (9, 28). Based on these findings, we postulate that GJ composed of Cx32 regulates ROS generation and distribution between renal cells, which then activates NF-κB/p53/PUMA-mediated mitochondrial apoptotic pathways, resulting in renal cell damage, contributing to IR-induced AKI aggravation.

This study not only further elucidates the role of Cx32 in IR-induced AKI but also explores its possible pathogenetic mechanism, thus providing a new mechanistic insight which could provide a basis for developing effective therapies to combat IR-induced AKI. We believe that this new finding could not only provide beneficial preventive measures for renal surgeries with IR injury but also beneficial for operations of other organ injury resulting from renal hypoperfusion caused by hypotension, such as liver transplantation, liver resection, cardiac surgeries, or operations requiring disruption of inferior vena caval patency.

Results

The changes of IR-induced renal injury and cell apoptosis were consistent with Cx32 expression alternation

Mice with similar weight (Supplementary Table S1) that underwent renal IR all survived at designated reperfusion time in our study and exhibited significant renal pathological damage as reperfusion time was extended, which reached peak activity at 24 h after reperfusion. Tubular necrosis, cell swelling and cytoplasm rarefaction, and inflammatory cells were observed at this critical time point, following which it recovered at 48 h after reperfusion (Fig. 1A, B). Changes of blood urea nitrogen (BUN) and creatinine (Cr) mirrored the patterns of pathological injury of kidney, reaching peak values at 24 h after reperfusion and recovering at 48 h (Fig. 1C, D).

FIG. 1. Increased renal damage and apoptosis were accompanied by enhanced renal expression of Cx32 protein in renal-IR-induced AKI. Male C57BL/6 mice that underwent renal IR were sacrificed at the time point of 6, 12, 24, and 48 h after reperfusion. Renal necrosis, renal tubular epithelial cells apoptosis, and Cx32 expression alternation were detected with different methods in kidneys. **(A)** Renal damage of mice at different reperfusion time points after renal IR (H&E; scale bar 50 μm). *Blue arrow*: tubular necrosis; *red arrow*: inflammatory cells; *black arrow*: cell swelling and cytoplasm rarefaction. **(B–D)** Kidney histopathology evaluation scores, levels of Cr and BUN at different reperfusion time points after renal IR. **(E)** Renal tubular epithelial cells apoptosis at different reperfusion time points after renal IR with TUNEL staining (scale bar 50 μm). **(F)** Renal Cx32 mRNA of mice at different reperfusion time points after renal IR with quantitative real-time polymerase chain reaction. **(G, H)** Renal Cx32 expression of mice at different reperfusion time points after renal IR with two different methods: Western blot analysis and IHC staining (scale bar 50 μm). Data are presented as mean ± SE ($n = 8$). $^{*}p < 0.05$ *versus* sham group; $^{\#}p < 0.05$ *versus* 24 h after reperfusion group **(F, G)**. AKI, acute kidney injury; BUN, blood urea nitrogen; Cr, creatinine; Cx32, connexin32; H&E, hematoxylin–eosin staining; IHC, immunohistochemistry; IR, ischemia reperfusion; TUNEL, terminal deoxynucleotidyl transferase dUTP nick-end labeling. Color images are available online.

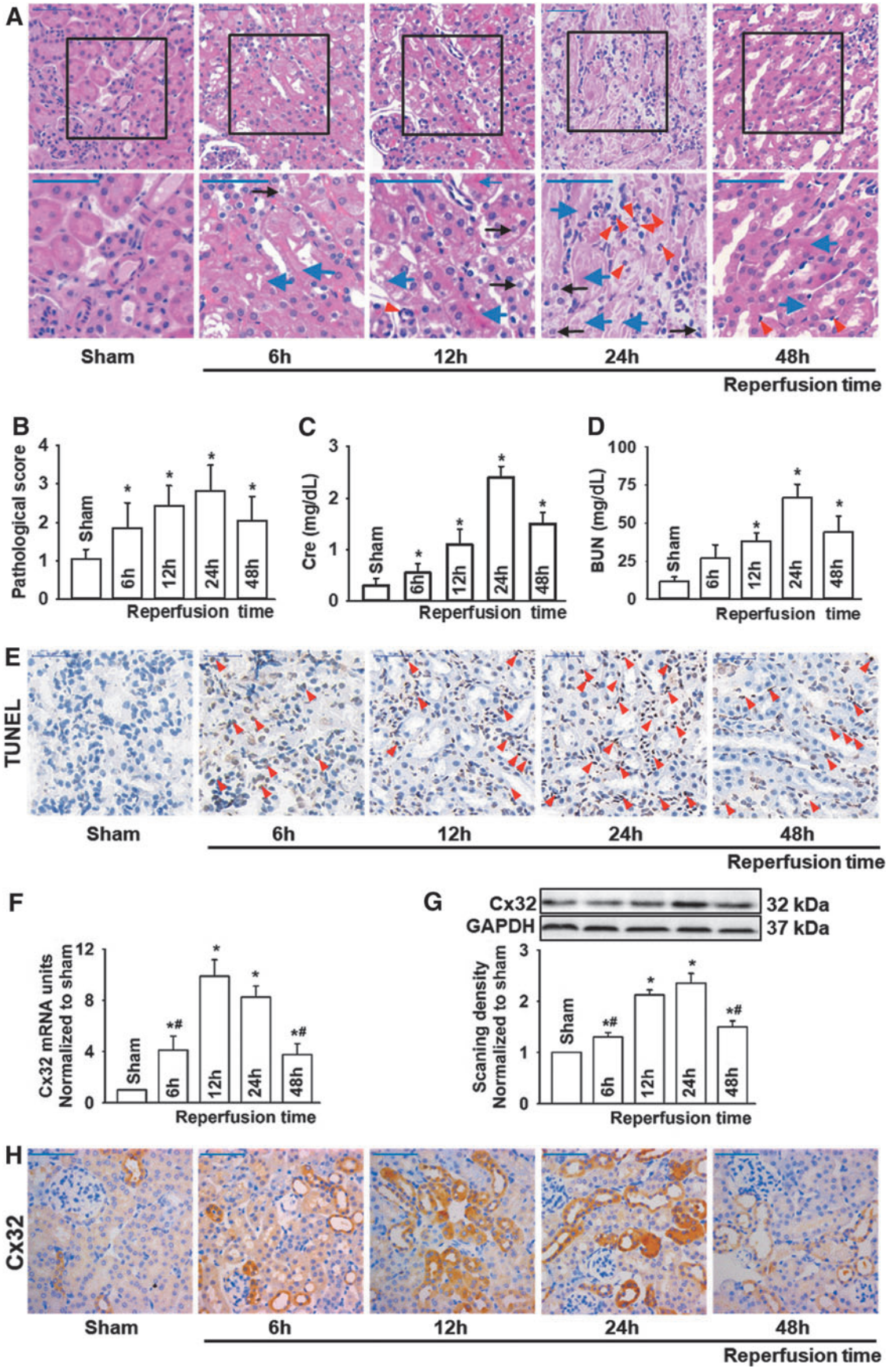
A
Sham
6h
12h
24h
48h
Reperfusion time
B
Pathological score
Reperfusion time
C
Cre (mg/dL)
Reperfusion time
D
BUN (mg/dL)
Reperfusion time
E
TUNEL
Sham
6h
12h
24h
48h
Reperfusion time
F
Cx32 mRNA units
Normalized to sham
Reperfusion time
G
Cx32
GAPDH
32 kDa
37 kDa
Scaning density
Normalized to sham
Reperfusion time
H
Cx32
Sham
6h
12h
24h
48h
Reperfusion time

These results suggested that renal injury induced by IR is a dynamic process. In addition, we observed that renal tissue apoptosis increased significantly when exposed to IR compared with sham group, and the number of apoptotic cells was the highest at 24 h after reperfusion (Fig. 1E), consistent with IR-induced renal injury, which prompted us to consider that apoptosis might be an important cause of IR-induced renal injury.

Twenty-one kinds of connexin (Cx) have been found in mammals, and at least 10 of them clearly expressed in renal tissues (1), among which the CX32 mRNA showed the greatest upregulation after IR (Supplementary Fig. S1).

As reported in our previous studies (22, 23), as Cx32 alternation-mediated liver transplantation-induced AKI was considered to be a new and vital therapeutic target for AKI, we used three different methods: polymerase chain reaction (PCR),

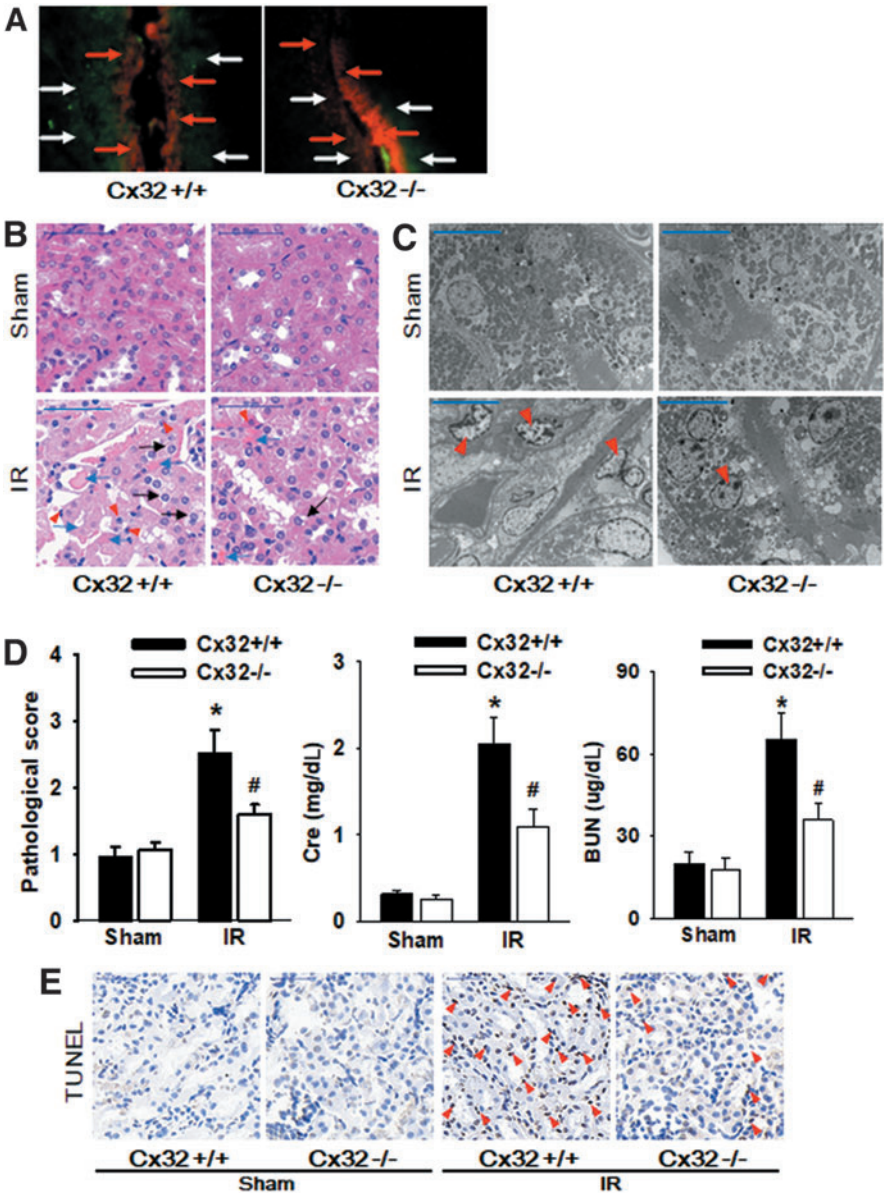

FIG. 2. Cx32 deficiency protects against IR-induced AKI and renal tubular epithelial cells apoptosis. $Cx32^{-/-}$ and $Cx32^{+/+}$ C57BL/6 mice underwent renal IR were sacrificed at the time point of 24 h after reperfusion. **(A)** ''Scrape-and-load'' assay was used to valuate functional GJ in kidney tissue. Function of GJ is demonstrated by the spread of GJ-permeable Lucifer yellow (*white arrow*), and in contrast Rhodamine is impermeable (*red arrow*). **(B)** Renal damage of $Cx32^{-/-}$ and $Cx32^{+/+}$ C57BL/6 mice after renal IR exposure (H&E; scale bar 50 μm). *Blue arrow*: tubular necrosis; *red arrow*: inflammatory cells; *black arrow*: cell swelling and cytoplasm rarefaction. **(C)** Ultrastructural mitochondrial injury of $Cx32^{-/-}$ and $Cx32^{+/+}$ C57BL/6 mice after renal IR exposure (TEM; scale bar 10 μm). *Red arrow*: cell nuclear condensation. **(D)** Kidney histopathology evaluation scores, levels of Cr and BUN of $Cx32^{-/-}$ and $Cx32^{+/+}$ C57BL/6 mice 24 h after renal IR. **(E)** Renal tubular epithelial cells apoptosis of $Cx32^{-/-}$ and $Cx32^{+/+}$ C57BL/6 mice 24 h after renal IR with TUNEL staining (scale bar 50 μm). Data are presented as mean ± SE ($n = 8$). $^{*}p < 0.05$ *versus* $Cx32^{+/+}$ sham group; $^{\#}p < 0.05$ *versus* $Cx32^{+/+}$ IR group in **(C)**. $Cx32^{-/-}$ mice, Cx32-gene knockdown mice; $Cx32^{+/+}$ mice, wild-type mice; GJ, gap junction; TEM, transmission electron microscopy. Color images are available online.

Western blotting, and immunohistochemistry, to determine Cx32 expression alternation. Results showed that both Cx32 mRNA and protein expression of renal tissues increased consistently at 12 or 24 h when subjected to IR. After that, these parameters gradually declined to base levels. The changes of renal Cx32 were also consistent with the patterns of pathological injury and apoptosis of kidney tissues (Fig. 1F–H).

Cx32 deficiency protects against IR-induced renal injury and cell apoptosis

To explore the role of Cx32 in IR-induced renal injury, Cx32 gene-deleted (Cx32-gene knockdown, $Cx32^{-/-}$) and kidney-specific Cx32 overexpression (Cx32-rAAV) were measured in C57BL/6 male mice ($n=8$ per group) to construct a model of renal IR. A "Scrape-and-load" *in vivo* assay was employed to detect functional changes of GJ composed of Cx32, and results indicated that dye spread was decreased significantly on kidney slices obtained from $Cx32^{-/-}$ mice (Fig. 2A).

More importantly, renal pathological damage, mitochondrial injury, Cr, BUN changes, and even the number of apoptotic cells following the treatment of renal IR were all decreased much more significantly than those from $Cx32^{+/+}$ (wild-type) mice (Fig. 2B–D). Results of Cx32-rAAV mice are shown in Supplementary Figure S2A–D. Cx32-rAAV significantly elevated Cx32 expression in mice kidney

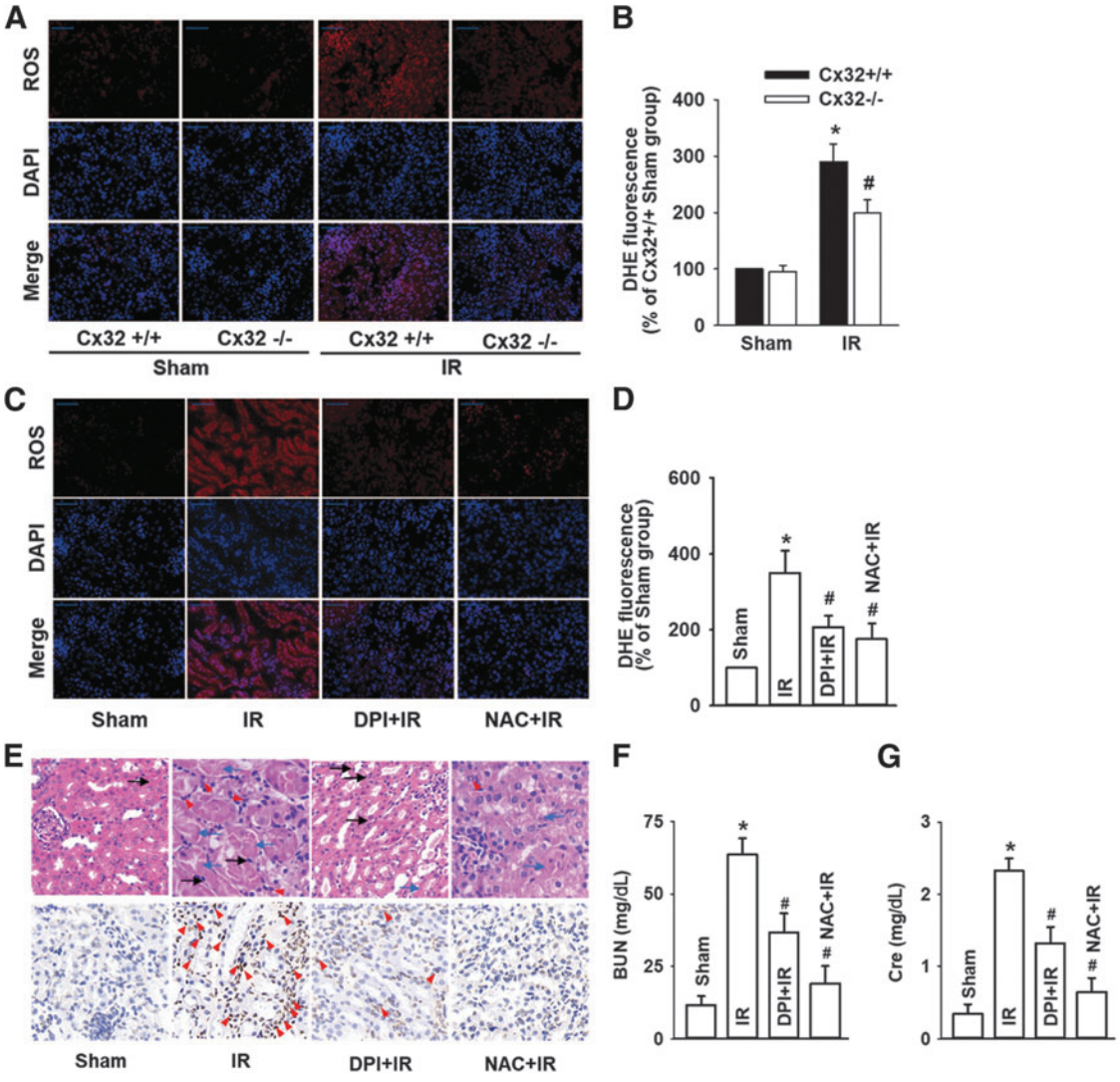

FIG. 3. Cx32 regulated the generation and distribution of ROS, which mediated IR-induced AKI. $Cx32^{-/-}$ and $Cx32^{+/+}$ C57BL/6 mice that underwent renal IR were sacrificed at the time point of 24 h after reperfusion. **(A, B)** Cx32 gene deletion resulted in significant decrease of renal IR-induced intercellular ROS production (ROS stained in *red* with DHE; cell nuclei stained in *blue* with DAPI). Values expressed as mean ± SE ($n=8$). $^{*}p<0.05$ compared with $Cx32^{+/+}$ Sham group; $^{\#}p<0.05$ *versus* $Cx32^{+/+}$ IR group. When mice were pretreated with DPI (inhibitor of NADPH oxidase, 100 mg/kg) or NAC (a ROS scavenger, 200 mg/kg) for 1 h before renal IR: **(C, D)** ROS production of renal tissues was decreased obviously (ROS stained in *red* with DHE; cell nuclei stained in *blue* with DAPI), **(E)** Kidney histopathology damage and renal tubular epithelial cells apoptosis were reduced obviously (H&E and TUNEL; scale bar 50 μm). **(F–G)** levels of Cr and BUN were all attenuated. Data are presented as mean ± SE ($n=8$). $^{*}p<0.05$ compared with Sham group; $^{\#}p<0.05$ *versus* IR group. DAPI, 6-diamino-2-phenylindole; DHE, dihydroethidium, DPI, diphenyleneiodonium chloride; NAC, N-acetyl cysteine; ROS, reactive oxygen species. Color images are available online.

tubules which suggested that Cx32 plays an important role in IR-induced renal injury, while its deficiency could protect against kidney damage and cells apoptosis.

Cx32 regulated the generation and distribution of ROS, which mediated IR-induced renal injury

Figures 1 and 2 demonstrated that Cx32 inhibition protected against IR-induced renal injury. However, the underlying mechanisms were still unknown. As ROS is just one of the few signals that can be transmitted through the channels of GJ, we measured changes of ROS generation and distribution when $Cx32^{+/+}$, $Cx32^{-/-}$, or Cx32-rAAV mice underwent IR injury. Results showed that although IR exposure resulted in an increase of ROS generation and distribution in kidney tissues, Cx32 deficiency attenuated and Cx32 overexpression enhanced these effects (Fig. 3A, B and Supplementary S3A). In addition, no significant changes in the expression of Cx32 and ROS were observed in other organs such as hearts and livers after renal IR, neither systemic knockdown nor kidney-specific overexpression of Cx32 altered ROS generation in hearts and livers after renal IR (Supplementary Fig. S3B).

These results suggested that the valid transfer path of ROS was suppressed with Cx32 deficiency and strengthened by Cx32 overexpression in kidneys after renal IR, which resulted in the reduction or induction of ROS generation and distribution, respectively. Next, we further investigated the effects of ROS on IR-induced renal injury with the use of two inhibitors (diphenyleneiodonium chloride [DPI], an inhibitor of NADPH oxidase; N-acetyl cysteine [NAC], a kind of ROS scavenger) to reduce the level of ROS in renal tissues. Results showed that both DPI and NAC not only effectively attenuated the increase of ROS resulted from IR injuries (Fig. 3C, D) but also concomitantly decreased IR-induced renal injury and apoptosis,

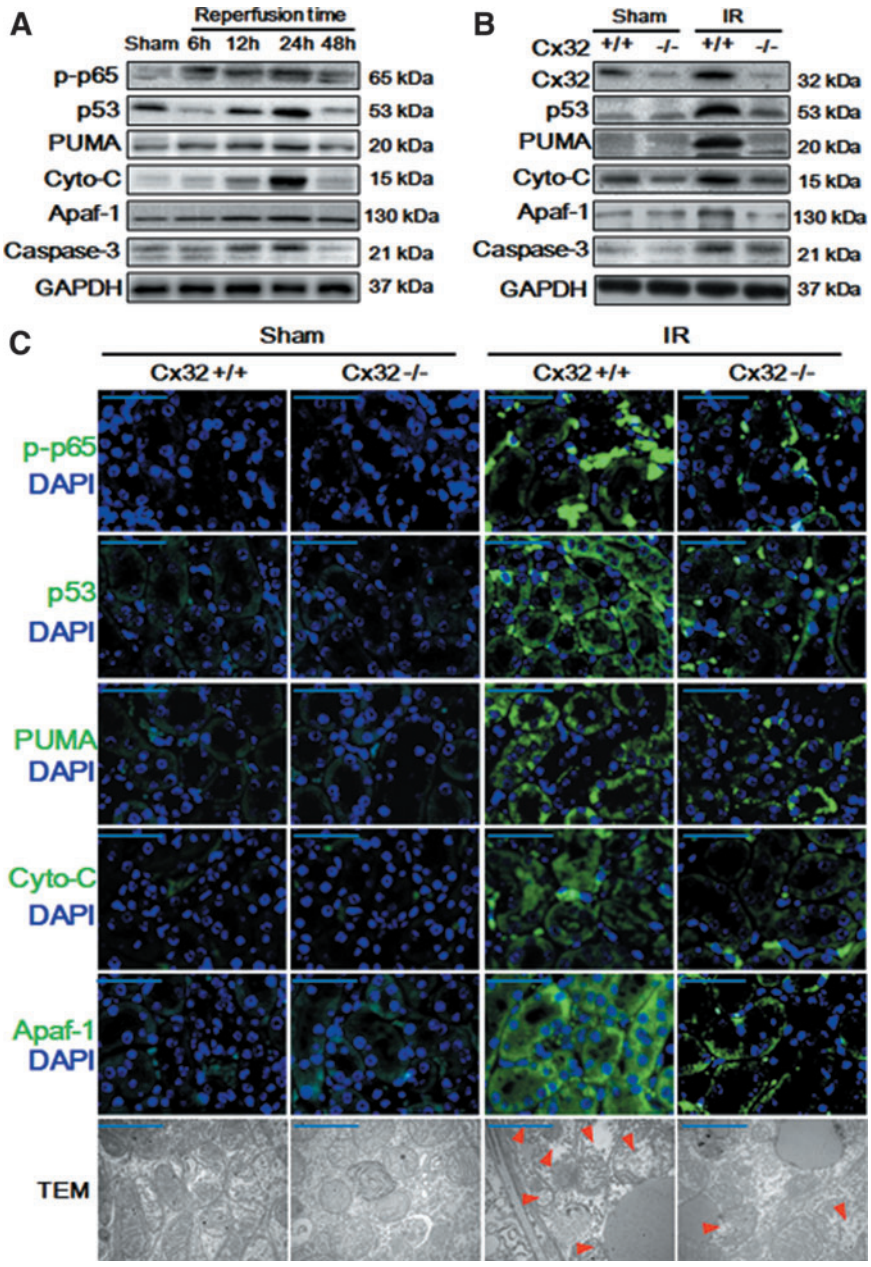

FIG. 4. Cx32 deficiency inhibited the activation of NF-κB/p53/PUMA-mediated mitochondrial apoptotic signaling pathways and mitochondrial injury after renal IR. (A) Dynamic changes of expression of mitochondrial-apoptosis-related protein by Western blot analysis at the time point of 6, 12, 24, and 48 h after reperfusion, including p-p65, p53, PUMA, cytochrome-C, Apaf-1, caspase-3 expression. **(B–C)** Cx32 gene deficiency attenuated the activation of NF-κB/p53/PUMA-mediated mitochondrial apoptotic signaling pathways at 24 h after reperfusion, manifested as the decrease of p-p65, p53, PUMA, cytochrome-C, Apaf-1, caspase-3 expression. [**(B)**, Western blot analysis; **(C)**, IF staining, target protein stained in *green* and cell nuclei stained in *blue* with DAPI, scale bar 50 μm; TEM images, scale bar 10 μm. *Red arrow*: mitochondrial edema and loss of inner membrane cristae]. Apaf-1, apoptotic protease activating factor-1; cyto-C, cytochrome C; IF, immunofluorescence; p-p65, phosphorylated p65 nuclear factor-κB; PUMA, p53 upregulated modulator of apoptosis. Color images are available online.

and were manifested as an improvement of the pathological injury, Cr, BUN, and the number of apoptotic cells (Fig. 3E–G).

Cx32 deficiency inhibited the activation of ROS-dependent NF-κB/p53/PUMA-mediated mitochondrial apoptotic signaling pathways and mitochondrial injury

It has been reported that ROS-mediated mitochondrial apoptosis might contribute to hydrogen peroxide (H_2O_2)-induced renal proximal tubule cellular damage (49, 53), and others have shown that ROS-dependent NF-κB and p53/PUMA activation pathways participated in cell apoptosis (7, 28). Although these conclusions are consistent with our findings that Cx32 regulate ROS generation and distribution in renal tissues (Fig. 3), we have reason to suggest that Cx32 could also manipulate the activation of NF-κB/p53/PUMA-mediated mitochondrial apoptotic signaling pathways through regulating ROS generation and distribution in kidneys.

Thus, Figure 4A illustrates our findings that as reperfusion time is extended, phosphorylated p65 nuclear factor-κB (p-p65), p53, PUMA, and mitochondrial apoptosis (manifested as cytochrome C, apoptotic protease activating factor-1 [Apaf-1], and caspase-3) were all gradually increased, and peaked at 12 or 24 h, coincident with the changes of IR-induced renal pathological damage and apoptosis (Fig. 1).

More importantly, when $Cx32^{-/-}$ mice underwent IR injury, Cx32 deficiency attenuated the IR-induced activation of NF-κB/p53/PUMA-mediated mitochondrial apoptotic

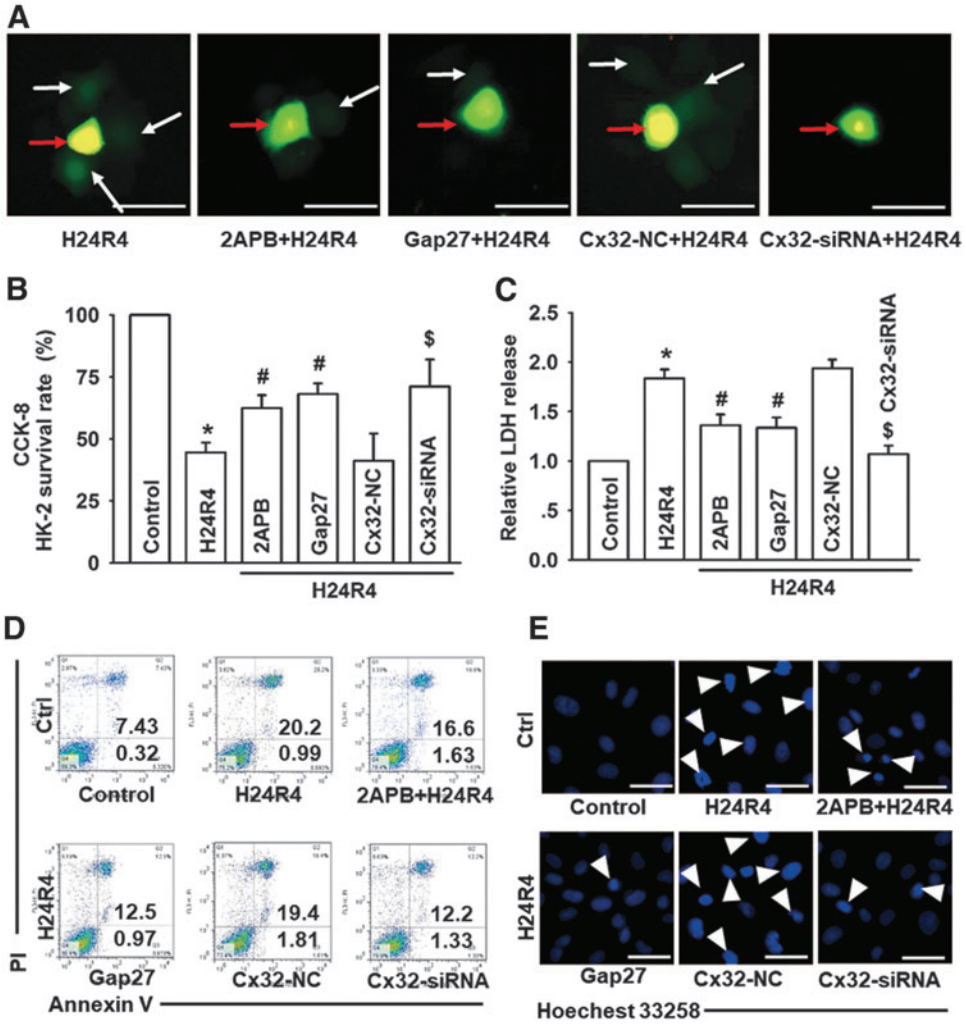

FIG. 5. Cx32 inhibition attenuated H24R4-induced cell injuries and apoptosis of HK-2 cells. Before H24R4 exposure, different methods were used to inhibit GJ function composed of Cx32 in HK-2 cells, including 2APB (gap junction inhibitor, 25 μM, 1 h pretreatment), Gap27 (Cx32 peptide, 100μM, 24 h pretreatment) and specific Cx32-siRNA, to observe effects of Cx32 GJ function on HK-2 cells damage and apoptosis. **(A)** ''Parachute'' dye-coupling assay was used to determine effects of 2-APB, Gap27, and Cx32-siRNA on decreasing GJ function (scale bar 50 μm). Function of GJ is demonstrated by the spread of GJ-permeable calcein-AM (*white arrow*), and in contrast CM-Dil is impermeable (*red arrow*). **(B, C)** Effects of 2APB, Gap27, and Cx32-siRNA on HK-2 cell growth and relative LDH release. **(D, E)** HK-2 cell apoptotic rates were detected by flow cytometry and Hoechst 33258 staining, as described in the Methods and Materials section. The *white arrow* **(E)** pointing the apoptotic nuclei. Data are presented as mean ± SE ($n = 4$). $^{*}p < 0.05$ compared with control group; $^{\#}p < 0.05$ *versus* H24R4 group. $^{\$}p < 0.05$ compared with Cx32-NC+H24R4 group in **(B–D)**. 2-APB, 2-aminoethoxydiphenyl borate; H24R4, hypoxia for 24 h and reoxygenation for 4 h; HK-2, human kidney tubular epithelial cell; LDH, lactate dehydrogenase. Color images are available online.

signaling pathways, manifested as the decrease of p-p65, p53, PUMA, cytochrome C, Apaf-1, and caspase-3 expression at 24 h after reperfusion with two different assays: Western blotting and immunofluorescence (Fig. 4B, C) and mitochondrial injury, manifested as normal mitochondrial shape and structure, and increase of Tfam, mitochondrial nucleoid factor 1 (MNF1) and Dynamin-related protein 1 (DRP1) expression (Fig. 4C and Supplementary Fig. S4). Therefore, we conclude that Cx32 affected IR-induced renal injury through regulating ROS-dependent NF-κB/p53/PUMA-mediated mitochondrial apoptotic signaling pathways.

Cx32 inhibition attenuated H24R4-induced injuries and apoptosis of renal proximal tubular epithelial cells

A separate set of investigations were dedicated to the construction of cell hypoxia for 24 h and reoxygenation for 4 h (H24R4) models with human kidney tubular epithelial

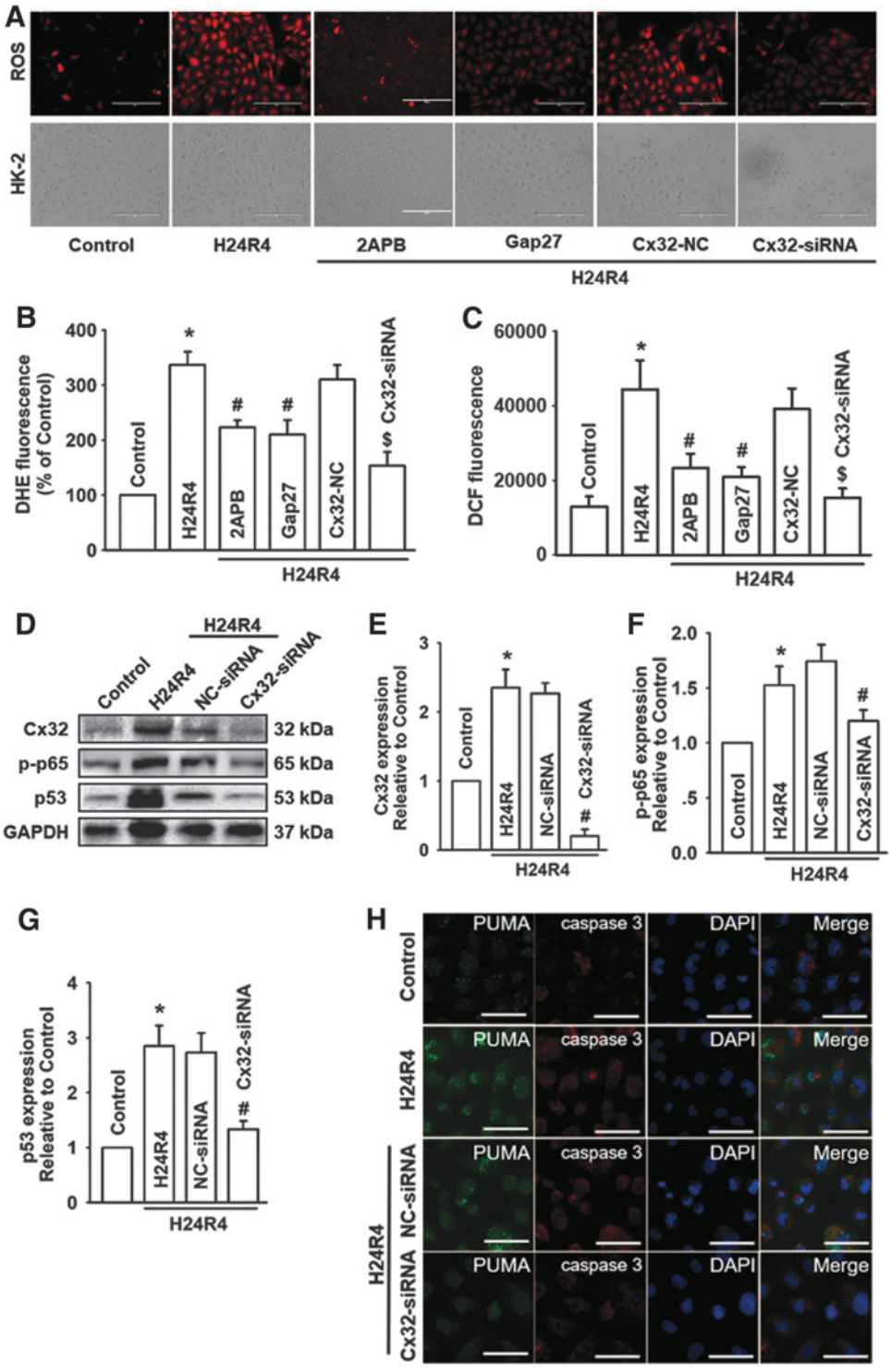

FIG. 6. Cx32 inhibition decreased H24R4-induced ROS generation and distribution, and attenuated the activation of NF-κB/p53/PUMA-mediated mitochondrial apoptosis in HK-2 cells. Before H24R4 exposure, different methods were used to inhibit GJ function composed of Cx32 in HK-2 cells, including 2APB (gap junction inhibitor, 25 μM, 1 h pretreatment), Gap27 (Cx32 peptide, 100 μM, 24 h pretreatment), and specific Cx32-siRNA, to observe effects of Cx32 GJ function on HK-2 cellular ROS production, and expression alternation of mitochondrial apoptosis-related proteins. **(A–C)** Effects of 2APB, Gap27, and Cx32-siRNA on HK-2 cellular ROS production, detected with DHE staining (**A, B,** stained in *red*, scale bar 50 μm) and DCFH-DA staining (**C**). **(D–G)** Effects of Cx32-siRNA on expression of Cx32, p-p65, and p53 in HK-2 cells with Western blot. **(H)** Effects of Cx32-siRNA on expression of PUMA and caspase-3 with IF staining (PUMA, stained in *green*; caspase-3, stained in *red*; cell nuclei, stained in *blue* with DAPI, scale bar 50 μm). Data are presented as mean ± SE ($n = 4$). $^{*}p < 0.05$ compared with control group; $^{\#}p < 0.05$ *versus* H24R4 group. $^{\$}p < 0.05$ compared with Cx32-NC+H24R4 group. DCFH-DA, 6-carboxy-2'-7'-dichlorodihydrofluorescein diacetate. Color images are available online.

cells (HK-2s) or rat kidney tubular epithelial cells (NRK52Es). First, to ensure the role of GJ in renal proximal tubular epithelial cells subjected to hypoxia reoxygenation (HR) *in vitro*, we have seeded the HK-2 cells at low density or high density to observe the effects of GJ on HR-induced ROS and mitochondrial apoptosis pathway changes, and we found that HR-induced ROS accumulation and mitochondrial apoptosis were density dependent, and low density of cells suffered less mitochondrial injury after HR (Supplementary Fig. S5A–G), indicating that GJ may play a critical role in ROS spread in injured renal proximal tubular epithelial cells *in vitro*.

Next, to confirm our findings that Cx32 deficiency could attenuate IR-induced renal damage and further delineate the possible mechanism for ROS-dependent NF-κB/p53/PUMA-mediated mitochondrial apoptosis, three methods with different mechanisms were utilized: 2-aminoethoxydiphenyl borate (2APB, a chemical inhibitor), Gap27 (a mimetic peptide), and Cx32-siRNA (target and knockdown Cx32 expression specifically) were used to inhibit GJ composed of Cx32.

Data showed that all the reagents for research had no significant influence on cell survival vitality (Supplementary Fig. S6A–D). A parachute assay showed that all of these methods could decrease the function of Cx32 GJ effectively (Fig. 5A and Supplementary Fig. S6E), and H24R4-induced cell damage (cell survival and lactate dehydrogenase [LDH] release) could be attenuated when HK-2 and NRK52E cells were pretreated with 2APB, Gap27, or Cx32-siRNA, manifested as the rate of cell survival increase and LDH release decrease (Fig. 5B, C and Supplementary Fig. S6F, G).

At the same time, flow cytometry and Hoechst 33258 staining were performed to investigate the effect of Cx32 on H24R4-induced cells apoptosis. Compared with the control group, apoptotic rates of both cells were almost increased

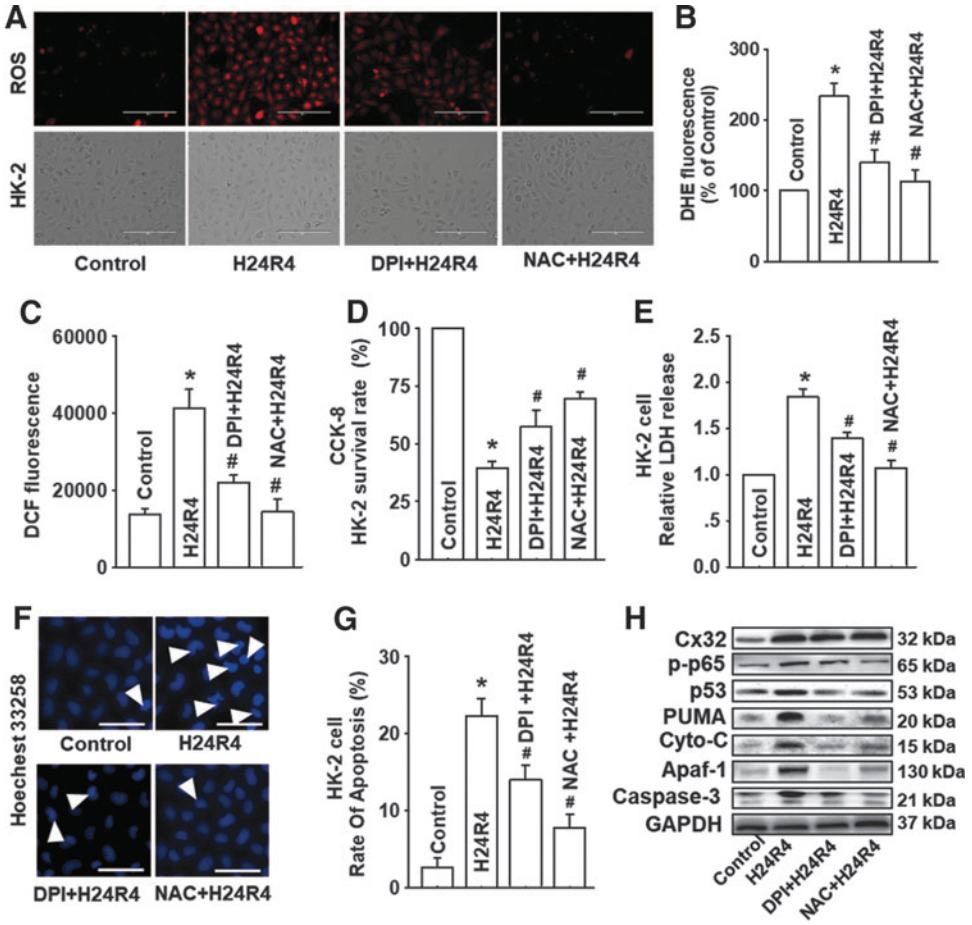

FIG. 7. Inhibitors of ROS, DPI, and NAC attenuated the activation of NF-κB/p53/PUMA-mediated mitochondrial apoptosis effectively, but had no influence on the expression of Cx32. Before H24R4 exposure, DPI (an inhibitor of NADPH oxidase, 1 μ*M*, 1 h pretreatment) and NAC (a ROS scavenger, 10 m*M*, 1 h pretreatment) were used to alter ROS generation and distribution, to observe effects of ROS on HK-2 cells damage and apoptosis, and even on expression alternation of mitochondrial apoptosis-related proteins. **(A–C)** Effects of DPI and NAC on HK-2 cellular ROS production after H24R4 exposure, detected with DHE staining **(A, B,** stained in *red*, scale bar 50 μm**)** and DCFH-DA staining **(C). (D, E)** Effects of DPI and NAC on HK-2 cell growth and relative LDH release after H24R4 exposure. **(F, G)** Effects of DPI and NAC on H24R4-induced HK-2 cell apoptosis, detected with Hoechst 33258 staining **(F**, *white arrow*: apoptotic nuclei, scale bar 50 μm**)** and flow cytometry **(G). (H)** DPI and NAC application attenuated expression of p-p65, p53, PUMA, cytochrome-C, Apaf-1, and caspase-3 after H24R4 exposure, but had no significant influence on Cx32 expression. Western blotting analysis was conducted. Data are presented as mean ± SE ($n = 4$). *$p < 0.05$ compared with control group; $^{\#}p < 0.05$ *versus* H24R4 group. NAC, N-acetyl cysteine. Color images are available online.

four times when exposed to H24R4 injury. However, this increase was depressed when Cx32 function was inhibited with 2APB, Gap27, or Cx32-siRNA. Studies *in vitro* demonstrated that Cx32 inhibition attenuated H24R4-induced injuries and apoptosis of renal proximal tubular epithelial cells (Fig. 5D, E and Supplementary Fig. S6H, I).

Cx32 inhibition decreased H24R4-induced ROS generation and distribution, and attenuated the activation of NF-κB/p53/PUMA-mediated apoptosis and mitochondrial injury

We demonstrated that Cx32 deficiency inhibited the activation of ROS-dependent NF-κB/p53/PUMA-mediated mitochondrial apoptosis *in vitro* (Fig. 3). Similarly, when function of Cx32 was inhibited with 2APB and Gap27, or knocked down by siRNA *in vitro*, H24R4-induced generation and distribution of ROS were both depressed significantly (Fig. 6A–C and Supplementary Fig. S7A–C). Meanwhile, H24R4-induced accumulation of mitochondrial ROS and reduction of mitochondrial membrane potential (MMP) were reversed significantly after Cx32 inhibition and deletion (Supplementary Fig. S7D–F).

Even more significant, Cx32 deficiency attenuated the H24R4-induced activation of NF-κB/p53/PUMA-mediated mitochondrial apoptosis, manifested as a decrease of p-p65, p53, PUMA, and caspase-3 expression with two different assays: Western blotting and immunofluorescence (Fig. 6D–H).

Inhibitors of ROS, DPI, and NAC attenuated the activation of NF-κB/p53/PUMA-mediated mitochondrial apoptosis effectively, but had no influence on the expression of Cx32

We have concluded that Cx32 could manipulate the activation of NF-κB/p53/PUMA-mediated mitochondrial apoptotic signaling pathways through regulating ROS generation and distribution *in vitvo*. To further extend and confirm these results, inhibitors of ROS, DPI, and NAC were used to reduce ROS generation and distribution on HK-2 and NRK52E cells. As ROS generation and distribution by H24R4 was depressed effectively (Fig. 7A–C and Supplementary Fig. S8A), H24R4-induced cell damage was reduced concomitantly as demonstrated by an increase of the cell survival rate and the decrease of LDH release (Figs. 7D, E and 8B–D).

In addition, pretreatment with DPI and NAC could alleviate H24R4-induced activation of NF-κB/p53/PUMA apoptotic signaling pathways (Fig. 7F–H). In contrast, we noticed that NAC and DPI had no effects on the expression of Cx32 (Fig. 7H), which suggested that both ROS and ROS-dependent NF-κB/p53/PUMA pathways are downstream of Cx32. The results shown in Figures 5–7 confirmed that Cx32 affected H24R4-induced HK-2 damage through regulating ROS-dependent NF-κB/p53/PUMA-mediated mitochondrial apoptotic signaling pathways.

Inhibition of NF-κB or p53 could depress H24R4-induced kidney tubular epithelial cell damage, but had no influence on the expression of Cx32

We have demonstrated that alternation of Cx32 could regulate the generation and distribution of ROS, which activated the NF-κB/p53/PUMA-mediated mitochondrial apoptotic signaling pathway. SN50 (a selective NF-κB nuclear translocation inhibitor) and pifithrin-α (PFT-α) (a selective inhibitor of p53), having no influence on cell survival (Fig. S6A–D), were used to inhibit the function of NF-κB or p53, respectively, to explore whether both of the inhibitors could significantly reduce H24R4-induced HK-2 damage and the number of apoptotic cells. Results indicated that both SN50 and PFT-α application could protect against H24R4-induced HK-2 or NRK52E cells damage, and decrease the number of apoptotic cells (Figs. 8A–F and Supplementary Fig. S9A–C).

We next explored the relationship between NF-κB and p53. Interestingly, SN50 (a NF-κB nuclear translocation inhibitor) application reduced H24R4-induced p-p65, p53, PUMA, and mitochondrial apoptosis (manifested as cytochrome C, Apaf-1, and caspase-3), but had no influence on the expression of Cx32; in contrast, PFT-α (a selective inhibitor of p53) application could also reduce H24R4-induced p53, PUMA, and mitochondrial apoptosis (manifested as cytochrome C, Apaf-1, and caspase-3), but had no influence on the expression of Cx32 and p-p65 (Fig. 8G–I and Supplementary Fig. S9D).

These results suggest that p53 was downstream of NF-κB. Therefore, it was validated in our research hypothesis that GJ composed of Cx32 is a key point in H24R4-induced kidney tubular epithelial cell damage, which manipulates ROS generation, and its downstream NF-κB/p53/PUMA-mediated mitochondrial apoptosis pathway.

Discussion

Although there are many studies directed at IR-induced AKI, the underlying mechanism of injury has not been fully understood so far (10).

In this investigation, we established *in vivo* murine renal IR models and HR models of HK-2 or NRK52E cells *in vitro*. Our results show that mice that underwent renal IR exhibited significant renal pathological damage as reperfusion time extended, which was consistent with the alternation of Cx32 expression. Cx32 deficiency could protect against IR-induced renal damage. More importantly, we found that IR-induced renal cell apoptosis mediated by Cx32 might be an important cause of renal injury, which could be relative with Cx32 manipulating ROS or its downstream NF-κB/p53/PUMA-mediated mitochondrial apoptosis pathway. Whether the inhibition of Cx32, ROS generation and distribution, or its downstream NF-κB/p53/PUMA-mediated mitochondrial apoptotic signaling pathway could improve IR-induced renal injury effectively needs further exploration.

Multifactorial pathogenetic factors were known to be involved in AKI (4, 8, 10, 17). In our previous study, we demonstrated that Cx32 inhibition attenuated liver transplantation-induced AKI; however, its underlying mechanism had not been explored very well (22). Thus, in this investigation, we further confirmed function of Cx32 on IR-induced AKI with $Cx32^{-/-}$ mice specifically, and explored in depth the possible mechanism.

Although it had been reported that 2APB could decrease function of Cx32 *in vivo* and *in vitro* dose dependently (30), it might have other nonspecific effects such as inhibiting receptors of IP3 and decreasing release of Ca^{2+} at high doses (25). Thus, in this study, our incorporation of the $Cx32^{-/-}$ and

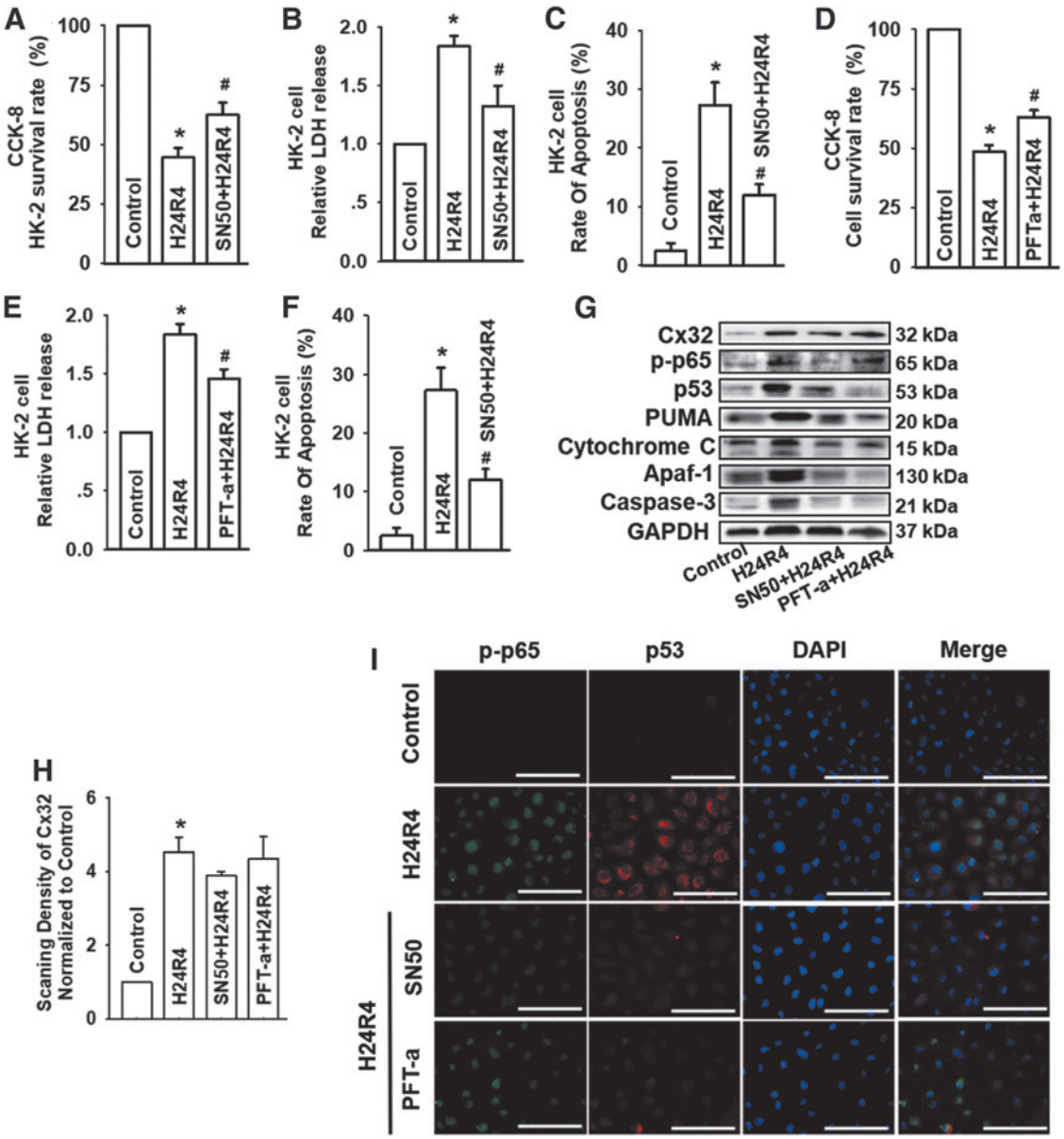

FIG. 8. Inhibition of NF-κB or p53 could depress H24R4-induced kidney tubular epithelial cell damage, but had no influence on the expression of Cx32. HK-2 cells were incubated with SN50 (a selective inhibitor of NF-κB, 20 μM) for 24 h or PFT-α (a selective inhibitor of p53, 10 μM) for 48 h before subjected to H24R4 treatment. **(A–C)** Effects of SN50 on HK-2 cell growth, LDH release, and apoptotic rate. **(D–F)** Effects of PFT-α on HK-2 cell growth, relative LDH release, and apoptotic rate. **(G, H)** Expression of Cx32, p-p65 and p53 and mitochondrial apoptosis-related protein, including PUMA, cytochrome-C, Apaf-1, and caspase-3, was detected by Western blot after H24R4 in HK-2 cells. **(I)** Expression of p-p65 and p53 was costained using IF (p-p65 was stained in *green* and p53 was stained in *red*, scale bar 50 μm). Data are presented as mean ± SE ($n = 4$). $^{*}p < 0.05$ compared with control group; $^{\#}p < 0.05$ *versus* H24R4 group. PFT-α, pifithrin-α. Color images are available online.

Cx32-rAAV mice, and use of Cx32 mimetic peptide and siRNA specifically to knock down or enhance Cx32 expression *in vitro* confirmed the role of Cx32 in mediating post-hypoxic cellular injury, which further confirmed our earlier observations (22).

From another aspect, we clarified that Cx32 manipulating ROS or its downstream NF-κB/p53/PUMA-mediated mitochondrial apoptosis pathway played a vital role in IR-induced renal damage for the first time. This new finding may not only be beneficial for renal surgeries with IR injury but could also have potential application for operations of other organs resulting in renal hypoperfusion caused by hypotension, such as liver transplantation, liver resection, cardiac surgeries, or operations requiring clipping of inferior vena cava. The elucidation of these mechanisms could provide new renal protection strategies.

As reported, GJ mediated the direct cell-to-cell transfer of electrical charge or small molecules, which contributed to cell growth, differentiation, normal physiology, and response to trauma in different kinds of organs. Molecular signaling

pathways that enhance cytotoxicity or apoptosis were called ''death signals'' (15, 18). Udawatte *et al.* (42) have revealed that apoptosis could spread from injured cells to other healthy neighboring cells, and the ''bystander effect'' was significantly reduced by blockage of Cx32 GJ. Even so, the actual events which translocate through GJs as ''death signals'' to induce apoptosis have not been established (18).

According to the characteristics of GJ, ROS is just one of the few signals that can be transmitted through the channels of GJ. Although the content of ROS (including oxygen radicals and nonradical compounds) in cells is very low, it still plays an important role in regulating physiologic tubular functions and renal microcirculation. Therefore, it is reasonable to conclude that increased ROS production and its distribution changes induced by IR *in vivo* or HR *in vitro* could lead to a series of severe damage effects, such as lipid peroxidation, structural integrity destruction, energy production disruption, and even high sensitivity of renal tubule to HR damage. Oxygen radicals or nonradical compounds could easily pass through GJ, for their molecular mass were much less than the upper limit of GJ permeable, which suggests that either or both oxygen radicals or nonradical compounds could provide ''death signals'' (11, 33).

In this investigation, it was clarified that ROS was accumulated in kidney cells after IR, and inhibition of GJ composed of Cx32 resulted in the alleviation of ROS generation or distribution, and further attenuated IR-induced AKI, which was consistent with reports that presence of Cx32 GJ increased the PDT phototoxicity in transfected HeLa cells and in the xenograft tumors through regulating ROS accumulation (13), and inhibition of ROS mediated by Cx32 could attenuate liver transplantation-induced renal damage (22).

Our investigation also demonstrated that DPI (inhibitor of NADPH oxidase) and NAC (a ROS scavenger) application alleviated IR-induced AKI and cell apoptosis through inhibiting NF-κB/p53/PUMA-mediated mitochondrial apoptosis pathway, but had no effects on the expression of Cx32, which indicated that ROS-dependent NF-κB/p53/PUMA pathway is downstream of Cx32.

As far as we know, NF-κB has always been considered to be an important transcription factor involved in the process of inflammation and apoptosis (24), which is normally sequestered in an inactive form in the cytoplasm bound to IκB proteins. Multiple stimuli can activate NF-κB signaling by degradation of IκB and release of the NF-κB p65–p50 dimer, which translocates to the nucleus and regulates transcriptional activation of the target genes (46). Some reports have demonstrated that NF-κB signaling pathway activation contributed to ROS-induced cell apoptosis. This phenomenon had been observed in different cells, such as human colorectal cancer cells (16), renal carcinoma cells (47), and ultraviolet B (UVB)-induced human keratinocyte cell injury (21).

Shimizu *et al.* reported that ROS increased NF-κB transcriptional activity and upregulated indoxyl sulfate-induced angiotensinogen expression in proximal tubular cells through promoting the phosphorylation of NF-κB p65, and NAC or DPI could suppress this effect (39). The present study also showed that DPI (inhibitor of NADPH oxidase) and NAC (a ROS scavenger) application effectively decreased NF-κB nuclear translocation induced by renal IR *in vivo* or H24R4 *in vitro*, and alleviated cell apoptosis and kidney injury. Based on these findings, we speculate that in renal tissues exposed to IR, ROS transferred through Cx32 GJ to activate the phosphorylation of NF-κB p65, and led to proximal tubular cells apoptosis and injury. Thus, we conclude that no matter inhibition of Cx32 GJ, ROS, or NF-κB signal pathway with different methods all could alleviate IR-induced renal damage.

Like NF-κB (p65), p53 is another important factor for cell apoptosis. Upregulation of p53 can induce renal cell apoptosis by stimulating the expression of PUMA, and p53/PUMA-induced mitochondrial apoptotic signaling pathway is always considered to be a key participant in the process of apoptosis after exposure to renal IR: apoptosis could be assuaged by PUMA inhibition, but exacerbated by PUMA enhancement (31, 50). Our study indicated that ROS-dependent NF-κB and p53/PUMA pathways activation participated in renal cells apoptosis induced by IR *in vivo* or H24R4 *in vitro*; however, the interaction between NF-κB and p53 varied significantly in different tissues and models.

It was reported that p53/PUMA-induced apoptosis was dependent on NF-κB activation in reovirus oncolysis of breast cancer (41) and high glucose-induced nascent nephron apoptosis (7). In contrast, others reported that in colon cancer cells, PUMA-induced apoptosis was motivated by p65 irrespective of p53 status (52), which was consistent with the earlier report that PUMA was directly activated by NF-κB in TNF-α-induced apoptosis (44).

Our study demonstrated that selective inhibition of NF-κB with SN50 reduced p65, p53, PUMA expression, and mitochondrial apoptosis induced by H24R4 (Fig. 8); and selective inhibition of p53 with PFT-α also reduced p53, PUMA expression, and mitochondrial apoptosis, but importantly had no influence on the expression and nuclear translocation of p65, indicating that p65 might regulate the activation of p53 and its downstream targets that PUMA-mediated mitochondrial apoptosis.

This study has some limitations which need to be considered: First, coincident with earlier reports, we found that there is no obvious expression of Cx32 in the glomerulus area, so we only focused on the renal tubular changes. However, it has been reported that renal IR might cause both the tubular and glomerular injuries (2, 38), hence further studies are now required to confirm our results, and the effect of Cx32 on the glomerular changes should be explored in the near future.

Second, the role of Cx32 varies in different tissues and different experimental models, here we only focus on the kidney tissue after renal IR; hence, a further study is needed to determine the potential role of Cx32 in other organs after IR in the future. Third, the role of Cx32 in mitochondrial apoptotic signaling pathway was clarified in this study; however, further study is needed to determine the role of Cx32 in other apoptotic pathways, including extrinsic and endoplasmic reticulum stress pathways.

In conclusion, we have conducted a series of *in vitro* and *in vivo* studies, and demonstrated that Cx32 plays a critical role in IR-induced AKI. GJ composed of Cx32 manipulated ROS generation and distribution between the neighboring cells, which altered activation of NF-κB/p53/PUMA-mediated mitochondrial apoptotic signaling pathways (Fig. 9). Cx32 function depression, ROS alleviation, or its downstream NF-κB/p53/PUMA-mediated mitochondrial apoptotic signaling pathways inhibition all could attenuate IR-induced AKI.

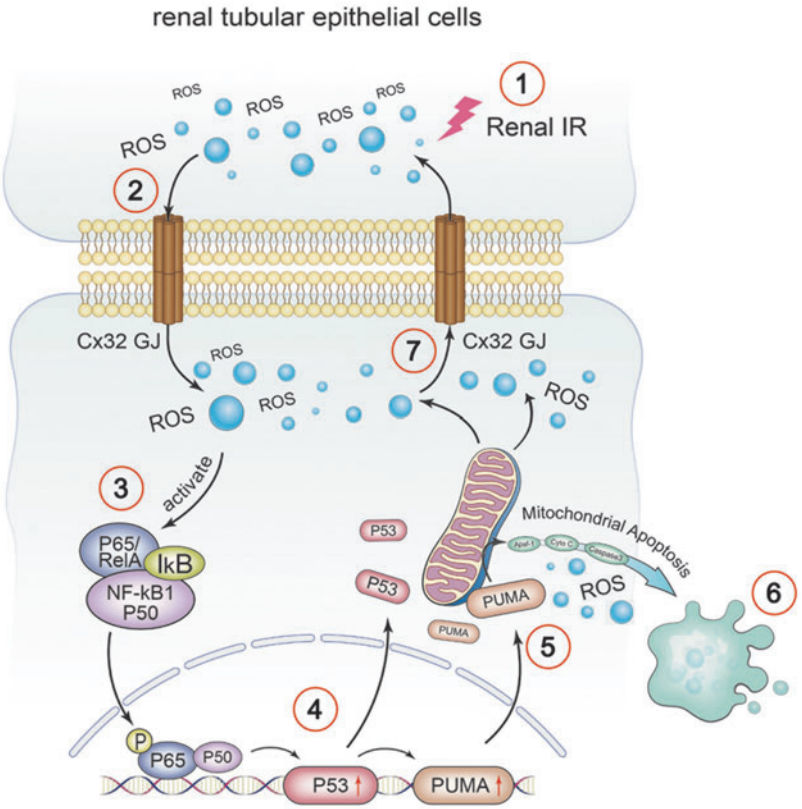

FIG. 9. Crosstalk between Connexin 32 and mitochondrial apoptotic signaling pathway in renal IR-induced AKI. In renal IR-induced AKI, Cx32 gap junction participated in cellular and renal damage by delivering ROS and activating NF-κB/p53/PUMA-mediated mitochondrial apoptotic signaling pathway. In the absence of Cx32, ROS production and accumulation are alleviated, which ameliorate p65 phosphorylation and p53/PUMA-induced cellular apoptosis and renal damage. Note: ①Step 1: renal IR causes the generation of ROS. ②Step 2: ROS is transmitted through GJ composed of Cx32. ③Step 3: ROS activates the NF-κB and causes p65 nuclear translocation. ④Step 4: p65 regulates the activation of p53 and its downstream targets, including PUMA. ⑤Step 5: activation of p53/PUMA induces mitochondrial apoptotic signaling pathway. ⑥Step 6: mitochondrial apoptosis occurs and gives rise to more ROS. ⑦Step 7: ROS is transmitted through GJ composed of Cx32 to another neighboring cell. Color images are available online.

This is the first description of the possible mechanism of Cx32 on renal IR-induced damage, which could provide multiple potential therapeutic targets for kidney protection, not only beneficial for renal surgeries with IR injury but also beneficial for operations of other organs resulting in renal hypoperfusion caused by hypotension, such as liver transplantation, liver resection, cardiac surgeries, or operations requiring clipping of inferior vena cava.

Materials and Methods

Materials

2APB, NAC, DPI, and dihydroethidium (DHE) were purchased from Sigma-Aldrich. Trizol reagent was purchased from Invitrogen. The ReverTra Ace quantitative real-time polymerase chain reaction (qPCR) RT Master Mix and SYBR® Green Realtime PCR Master Mix were purchased from TOYOBO. The Situ Cell Death Detection kit and the LDH assay kit were provided by Roche. The ROS assay kit and the JC-1 assay kit were purchased from Beyotime (Nanjin, China). MitoSOX Red Mitochondrial Superoxide Indicator was purchased from Yeasen (Shanghai, China). Fetal bovine serum (FBS) was purchased from Gibco.

Cx32 peptide 32Gap27 (SRPTEKTVFT) was purchased from GenScript. PFT-α was purchased from Selleck. SN50 was purchased from Alexis. Cx32-siRNA were commercially obtained from Biomics. The Lipofectamine® 3000 transfection reagent was purchased from Life technology. CCK-8 assay kit and Annexin V-FITC tip were purchased from KeyGEN Biotech. Recombinant adeno-associated virus (rAAV) vectors were offered by Genechem (Shanghai, China).

Animals and treatment

Experimental protocols and design were approved by the Institutional Animal Care and Use Committee at The Third Affiliated Hospital of Sun Yat-Sen University (Guangzhou, Guangdong province, China). Animal care was conducted in accordance with the Guidelines of Sun Yat-sen University for Animal Experimentation. Eight- to 10-week-old C57BL/6 male mice (20–25 g) were used for our experiments. The mice were maintained in microisolator cages under standard conditions (room temperature at 25–27°C with 12-h light/dark cycle), and allowed free access to specific pathogen-free laboratory food and distilled water.

$Cx32^{+/-}$ mice (European Mouse Mutant Archive, ID:00243, Italy) in the C57BL/6 background were used to generate $Cx32^{+/+}$ and $Cx32^{-/-}$ littermates. As previously described, genotyping was performed by PCR using genomic DNA extracted from tail snip (27). The kidney-specific Cx32 overexpression mice were constructed by tail vein injection of rAAV vectors containing the genes for Cx32 according to an earlier report (34).

The mice were randomly assigned to five groups ($n=8$ per group) in the initial intervention model establishment study, which included sham-operated, reperfusion 6-, 12-, 24-, and 48-h groups. Subsequent *in vivo* studies were performed using the 24-h reperfusion renal IR model. The $Cx32^{+/+}$, $Cx32^{-/-}$, and Cx32-rAAV mice were then randomly assigned to six groups ($n=8$ per group) to explore the role of GJ function in renal IR injury, including $Cx32^{+/+}$ sham, $Cx32^{+/+}$ IR, $Cx32^{-/-}$ sham, $Cx32^{-/-}$ IR, Cx32-rAAV sham, and Cx32-rAAV IR groups. Before operation, mice were treated intraperitoneally with DPI at doses 100 mg/kg for 1 h or with NAC at doses 200 mg/kg for 1 h before renal IR.

Tail vein injection of rAAV vectors

A kidney-specific Cx32 overexpression model was constructed with C57BL/6J mice by tail vein injection of rAAV vectors containing the genes for Cx32 (Genbank ID NM_001302496; Genechem, Shanghai, China) according to an earlier report (34). In brief, 1×1012 vg rAAV 2/9-CMV-eGFP were diluted into 200 μL saline and injected through tail vein at 4 weeks of life. The AAV vector expressing green fluorescence protein only was used as a negative control. At 4 weeks post injection, the animals were sacrificed.

Renal IR model

To minimize experimenter bias, the operator was blinded to the treatment conditions. All the mice were anesthetized by intraperitoneal injections of ketamine (60 mg/kg), then undertook bilateral renal pedicle clamping for 45 min and reperfusion for the indicated time. The sham group was identical to the surgery manner without renal pedicle occlusion. To maintain body temperature stable at 37°C during surgery, a heating pad was used. After operation, the mice were housed in microisolator cages, and allowed free access to water and chow. After designated reperfusion time, mice were sacrificed, blood and the kidneys were collected for further experiments.

Quantitative real-time PCR

Total RNA extracted from snap-frozen renal tissues were isolated using Trizol reagent. For the detection of RNA quality and concentration, we used a NanoDrop-1000 spectrophotometer. Reverse transcription was performed using ReverTra Ace qPCR RT Master Mix. Quantitative analysis of Cx32 mRNA, mitochondrial transcription factor A (Tfam), MNF1, and DRP1 was conducted with qPCR using SYBR Green Realtime PCR Master Mix with Roche LightCycler 1.1. GAPDH was used as the housekeeping gene. All the samples were tested in quadruple, and differences of threshold cycles (CT) between the target genes and GAPDH were calculated with the $2^{-\Delta\Delta CT}$ method and normalized to sham group.

BUN and Cr measurement

Blood samples were drawn from inferior vena cava at designated reperfusion time. After clotting at room temperature for 30 min, serum was isolated from blood by centrifugation (7500 rpm at 4°C for 10 min). BUN and Cr were analyzed using an automatic biochemistry analyzer (Watford Olympus AU640, United Kingdom), according to manufacturer's instructions.

"Scrape-and-load" assay. GJ function composed of Cx32 was detected by ''Scrape-and-load'' assay *in vivo* as earlier described (22). Kidneys were excised and freshly sliced 24 h after reperfusion. A 27-gauge needle was then placed into a solution containing 0.5% Rhodamine and Lucifer Yellow, and mechanically dipped into each kidney slice for 5-min dye incubation. Kidney slices were then cut into 5-μm frozen sections and imaged by fluorescence microscopy. Function of GJ was calculated by the distance of dye spread between the dye transfer front and the scrape line.

Hematoxylin–eosin staining and TUNEL assay

Kidneys were fixed in 10% buffered formalin overnight at 4°C, and then embedded in paraffin. Kidney sections that have been cut into 5 μm were used for several purposes. One section was for histopathological analysis using hematoxylin–eosin staining (H&E). Tubular injuries, including renal tubule dilation, tubular epithelial injury, and cast formation, were graded with a score of 0–4 (0, no change; 1, change affecting <25% of the field; 2, change affecting 25–50% of the field; 3, change affecting 50–75% of the field; 4, change affecting >75% of the field) (6). Another section for apoptosis was detected by terminal deoxynucleotidyl transferase dUTP nick-end labeling (TUNEL) assay with the In Situ Cell Death Detection kit following the manufacturer's instructions.

Transmission electronic microscopy analysis

Transmission electronic microscopy analysis was performed to observe the morphology of renal tubular cell nucleus and mitochondria. Fresh kidney tissue was rapidly removed after sacrificing the mice, and washed with phosphate-buffered saline (PBS, pH 7.4) and fixed with 2.5% glutaraldehyde overnight. After washing with PBS, the samples were dehydrated and embedded in Durcupan resin (Sigma-Aldrich). Ultrathin sections were cut and observed with a HT7700 transmission electron microscope (Hitachi, Japan).

Detection of rat kidney tissue ROS production

Levels of *in situ* ROS production were detected by DHE staining as described (20). Frozen sections of kidney tissue of 5 μm thick were incubated with 7.5-mM DHE at 37°C for 30 min. All fluorescence images were examined using a EVOS FL fluorescence microscope (EVOS FL, Life Technology). The fluorescence of DHE-labeled positive nuclei in 10 randomly selected fields of each sample is calculated, and is expressed as a percentage of the DHE-stained positive cell nuclei compared with control by a quantitative morphometric method (14).

Cell culture

NRK52E cell and HK-2 cell were obtained from American Tissue Culture Collection, and cultured in Dulbecco's Modified Eagle's medium (DMEM) containing 10% FBS. Cells were grown at 37°C in a humidified atmosphere with 5% CO_2 in air at 37°C.

Cell treatment

The NRK52E and HK-2 cell HR model was performed to mimic renal IR injury as previously described (22). Cells were seeded at low density (25,000 cells/cm^2, no GJ formed) or high density (125,000 cells/cm^2, GJ formed) in 24-well cell culture plates as previously described (22). Seventy to 80% of confluent cells were incubated in low-glucose and serum-deprived DMEM under low oxygen (1% O_2) for 24 h in a humidified hypoxia incubator, and then transferred back to normal oxygen (95% air +5% CO_2) for 4 h. The cells were pretreated with 2APB (connexin channel inhibitors), 25 μM, for 1 h; 32Gap27 (a Cx32 peptide), 100 μM, for 24 h, DPI (an inhibitor of NADPH oxidase), 1 μM for 1 h and NAC (a ROS scavenger), 10 mM for 1 h, PFT-α (a p53 inhibitor), 10 μM,

for 48 h, SN50 (an inhibitory peptide of NF-κB), 20 μM, for 24 h before inducing HR injury.

Inhibition of Cx32 expression by si-RNA transfection

Cx32-siRNA (CACCAACAACACATAGAAA) duplexes targeting Cx32 rat gene (GenBank accession ID: AY074717.1) and Cx32-siRNA (GAAGAGGUAUUGAAUGCUA) duplexes targeting Cx32 human gene (NCBI Gene ID: 2705) were used to silence Cx32 expression. A nonspecific siRNA was taken as siRNA control (NC group). Transfection into NRK52E and HK-2 cells was carried out using Lipofectamine 3000 transfection reagent following the manufacturer's instructions.

"Parachute" dye-coupling assay

GJ function was examined with ''Parachute'' dye-coupling assay *in vitro* as described (30, 43). Cells were grown to confluence in 12-well cell culture plates. Donor cells from one well were incubated with a freshly made solution of 10 μg/mL calcein-AM and 5 μg/mL CM-Dil in growth medium for 30 min, at 37°C and pH 7.4. CM-Dil is a membrane dye that does not spread to coupled cells. Calcein-AM is converted intracellularly into the GJ-permeable dye calcein. Unincorporated dye was removed by three consecutive washes with culture medium. The donor cells were then trypsinized and seeded onto the receiver cells at a 1:150 donor/receiver ratio.

The cells were allowed to attach to the monolayer of receiver cells and form GJs for 4 h at 37°C and pH 7.4, and then examined with a fluorescence microscope (EVOS FL, Life Technology). The average number of receiver cells containing calcein per donor cell was considered as a measure of the degree of gap junctional intercellular communication (GJIC).

Cell viability and cytotoxicity assay

HK-2 and NRK52E cells were planted in 96-well cell culture plates at a density of 5000 cells/well. At the end of different stimulation, the cell viability and LDH release *in vitro* were tested using a CCK-8 assay kit and an LDH assay kit according to the manufacturer's introduction using a microplate reader.

Annexin V-FITC/propidium lode staining

Cells were collected 4 h after reoxygenation. For analysis of apoptosis by flow cytometry, cells were stained by Annexin V-FITC and counterstained by propidium lode, and then analyzed by flow cytometry following the manufacturer's instructions. Data analysis was conducted by FlowJo 7.6.5 (TreeStar) software.

Hoechst 33258 stains

Cells were seeded on sterile cover glasses placed in the 24-well cell culture plates and accepted HR model. For nuclear staining, cells were fixed with 4% paraformaldehyde and stained with 2-μg/mL Hoechst 33258. Stained cells were observed under a fluorescence microscope. Morphological changes in typical nuclear fragmentation and chromatin condensation were used to characterize apoptosis cells. The percentage of apoptosis was calculated from the amount of apoptosis nuclei *versus* the total number of nuclei in each visual field.

ROS detection in cultured proximal tubule epithelial cells

ROS detection was conducted using three methods. Cells planted in 24-well cell culture plates were subjected to HR protocol. After reoxygenation for 4 h, cells were washed twice with PBS and incubated in the presence of 10-μM DHE in serum-free DMEM for 30 min at 37°C. Meanwhile, mitochondrial superoxide formation was detected by incubating cells in the dark with MitoSOX Red dye (5 μM) for 10 min at 37°C. Stains of intracellular ROS are observed in 10 randomly selected fields of each sample under a fluorescence microscope (EVOS FL, Life Technology), and are expressed as a percentage of the DHE-stained positive cells compared with control by a quantitative morphometric method (14).

Other cells collected 4 h after reoxygenation were stained with the ROS assay kit (6-carboxy-2'-7'-dichlorodihydrofluorescein diacetate [DCFH-DA]), and then detected by flow cytometry, and the fluorescence intensity of cells for each group was calculated following the manufacturer's instructions.

Measurement of mitochondrial membrane potential

MMP was determined by an MMP assay kit with JC-1 (Beyotime, Nanjing, China). In brief, cells were cultured and subjected to HR protocol. After reoxygenation for 4 h, cells were collected, washed, and resuspended in DMEM, and then incubated with the same volume of JC-1 working solution at 37°C for 20 min. After that, cells were centrifuged, washed, and resuspended in JC-1 dyeing buffer, and then analyzed by flow cytometry following the manufacturer's instructions. Data analysis was conducted by FlowJo 7.6.5 (TreeStar) software.

Immunofluorescence and immunohistochemistry

IR-injured kidney sections of 5-μm thick embedded in paraffin, and cells planted in sterile cover glasses and then subjected to HR protocol were prepared for immunofluorescence. The samples were stained with the following antibodies: p-p65, p53 (1:100; CST); PUMA (1:1000, Abcam); Caspase 3 (1:50, Santa Cruz Biotechnology) at 4°C overnight, followed by antirabbit or antimouse IgG (1:1000) according to the manufacturer's instruction. Cell nuclei were stained with 6-diamino-2-phenylindole (DAPI). All images were examined using a EVOS FL fluorescence microscope (EVOS FL, Life Technology), and 10 randomly selected fields of each sample were semiquantified.

Immunohistochemical staining was performed to detect the expression of Cx32 in kidney sections embedded in paraffin with Cx32 Antibody (1:50, Novus).

Western blot analysis

Western blotting follows the standard procedures as described (26) with the use of the following antibodies: Cx32 (1:3000; Sigma-Aldrich); p-p65, p53 (1:1000; CST); PUMA (1:1000, Abcam); Caspase 3, Cytochrome C, Apaf-1 (1:500, Santa Cruz Biotechnology), and GAPDH (1:5000, Proteintech). All Western blots were repeated at least thrice. Images were acquired by Tanon 5500 imaging system (Tanon, Shanghai). The images were scanned with the ImageJ scanning software; the data are

expressed as the values relative to the sham or control value. All the Western blot bands are shown in Supplementary Fig. S10.

Statistical analysis

Statistical analysis was performed using *SPSS 13.0* (SPSS, Inc., Chicago, IL) and Sigmaplot 10.0 (Systat Software, Inc., Chicago, IL). Kolmogorov–Smirnov test was used to test the normality of the data. Multiple comparisons among different groups were made using one-way analysis of variance (ANOVA), followed by Tukey's post hoc test. Quantitative data are presented as mean ± SE. The p-values <0.05 were considered statistically significantly different.

Acknowledgments

This study is supported by the National Natural Science Foundation of China (Grant No. 81571926; 81401628; 81372090; 81772127; 81601724); Science and Technology Project of Guangdong Province (Grant No. 2013B051000035); Guangzhou Science and Technology Plan (Grant No. 2015 08030003; 2016A020220010; 201607010233); Outstanding Young Teacher Training Program of Sun Yat-sen University, China (Grant No. 17ykpy55). We thank Prof. Zhengyuan Xia for his insightful guidance in the experimental design. We also thank Prof. Song G Zheng, professor and director at Penn State University, and Prof. Joseph A. Bellanti from Departments of Pediatrics and Microbiology-Immunology in Georgetown University Medical Center for their further edition of our MS revision.

Author Disclosure Statement

No competing financial interests exist.

References

1. Abed AB, Kavvadas P, and Chadjichristos CE. Functional roles of connexins and pannexins in the kidney. *Cell Mol Life Sci CMLS* 72: 2869–2877, 2015.
2. Andersson M, Nilsson U, Hjalmarsson C, Haraldsson B, and Nystrom JS. Mild renal ischemia-reperfusion reduces charge and size selectivity of the glomerular barrier. *Am J Physiol Ren Physiol* 292: F1802–F1809, 2007.
3. Aronson S, Phillips-Bute B, Stafford-Smith M, Fontes M, Gaca J, Mathew JP, and Newman MF. The association of postcardiac surgery acute kidney injury with intraoperative systolic blood pressure hypotension. *Anesthesiol Res Pract* 2013: 174091, 2013.
4. Bonventre JV and Yang L. Cellular pathophysiology of ischemic acute kidney injury. *J Clin Invest* 121: 4210–4221, 2011.
5. Cavaille-Coll M, Bala S, Velidedeoglu E, Hernandez A, Archdeacon P, Gonzalez G, Neuland C, Meyer J, and Albrecht R. Summary of FDA workshop on ischemia reperfusion injury in kidney transplantation. *Am J Transplant* 13: 1134–1148, 2013.
6. Chen BL, Sheu ML, Tsai KS, Lan KC, Guan SS, Wu CT, Chen LP, Hung KY, Huang JW, Chiang CK, and Liu SH. CCAAT-enhancer-binding protein homologous protein deficiency attenuates oxidative stress and renal ischemia-reperfusion injury. *Antioxid Redox Signal* 23: 1233–1245, 2015.
7. Chen YW, Chenier I, Chang SY, Tran S, Ingelfinger JR, and Zhang SL. High glucose promotes nascent nephron apoptosis via NF-kappaB and p53 pathways. *Am J Physiol Ren Physiol* 300: F147–F156, 2011.
8. Chuang ST, Kuo YH, and Su MJ. Antifibrotic effects of KS370G, a caffeamide derivative, in renal ischemia-reperfusion injured mice and renal tubular epithelial cells. *Sci Rep* 4: 5814, 2014.
9. Dai Y, Rahmani M, Dent P, and Grant S. Blockade of histone deacetylase inhibitor-induced RelA/p65 acetylation and NF-kappaB activation potentiates apoptosis in leukemia cells through a process mediated by oxidative damage, XIAP downregulation, and c-Jun N-terminal kinase 1 activation. *Mol Cell Biol* 25: 5429–5444, 2005.
10. Devarajan P. Update on mechanisms of ischemic acute kidney injury. *J Am Soc Nephrol* 17: 1503–1520, 2006.
11. Du K, Williams CD, McGill MR, Xie Y, Farhood A, Vinken M, and Jaeschke H. The gap junction inhibitor 2-aminoethoxy-diphenyl-borate protects against acetaminophen hepatotoxicity by inhibiting cytochrome P450 enzymes and c-jun N-terminal kinase activation. *Toxicol Appl Pharmacol* 273: 484–491, 2013.
12. Eltzschig HK and Eckle T. Ischemia and reperfusion–from mechanism to translation. *Nat Med* 17: 1391–1401, 2011.
13. Farmer EE and Mueller MJ. ROS-mediated lipid peroxidation and RES-activated signaling. *Annu Rev Plant Biol* 64: 429–450, 2013.
14. Fiordaliso F, Bianchi R, Staszewsky L, Cuccovillo I, Doni M, Laragione T, Salio M, Savino C, Melucci S, Santangelo F, Scanziani E, Masson S, Ghezzi P, and Latini R. Antioxidant treatment attenuates hyperglycemia-induced cardiomyocyte death in rats. *J Mol Cell Cardiol* 37: 959–968, 2004.
15. Hong X, Wang Q, Yang Y, Zheng S, Tong X, Zhang S, Tao L, and Harris AL. Gap junctions propagate opposite effects in normal and tumor testicular cells in response to cisplatin. *Cancer Lett* 317: 165–171, 2012.
16. Jeong JB, Choi J, Baek SJ, and Lee SH. Reactive oxygen species mediate tolfenamic acid-induced apoptosis in human colorectal cancer cells. *Arch Biochem Biophys* 537: 168–175, 2013.
17. Khan M, Yi F, Rasul A, Li T, Wang N, Gao H, Gao R, and Ma T. Alantolactone induces apoptosis in glioblastoma cells via GSH depletion, ROS generation, and mitochondrial dysfunction. *IUBMB Life* 64: 783–794, 2012.
18. Krutovskikh VA, Piccoli C, and Yamasaki H. Gap junction intercellular communication propagates cell death in cancerous cells. *Oncogene* 21: 1989–1999, 2002.
19. L'Hoste S, Chargui A, Belfodil R, Duranton C, Rubera I, Mograbi B, Poujeol C, Tauc M, and Poujeol P. CFTR mediates cadmium-induced apoptosis through modulation of ROS level in mouse proximal tubule cells. *Free Radic Biol Med* 46: 1017–1031, 2009.
20. Li H, Yao W, Irwin MG, Wang T, Wang S, Zhang L, and Xia Z. Adiponectin ameliorates hyperglycemia-induced cardiac hypertrophy and dysfunction by concomitantly activating Nrf2 and Brg1. *Free Radic Biol Med* 84: 311–321, 2015.
21. Liu X, Shi S, Ye J, Liu L, Sun M, and Wang C. Effect of polypeptide from Chlamys farreri on UVB-induced ROS/NF-kappaB/COX-2 activation and apoptosis in HaCaT cells. *J photochem photobiol B Biol* 96: 109–116, 2009.
22. Luo C, Yuan D, Li X, Yao W, Luo G, Chi X, Li H, Irwin MG, Xia Z, and Hei Z. Propofol attenuated acute kidney injury after orthotopic liver transplantation via inhibiting gap junction composed of connexin 32. *Anesthesiology* 122: 72–86, 2015.

23. Luo C, Yuan D, Yao W, Cai J, Zhou S, Zhang Y, and Hei Z. Dexmedetomidine protects against apoptosis induced by hypoxia/reoxygenation through the inhibition of gap junctions in NRK-52E cells. *Life Sci* 122: 72–77, 2015.
24. Marko L, Vigolo E, Hinze C, Park JK, Roel G, Balogh A, Choi M, Wubken A, Cording J, Blasig IE, Luft FC, Scheidereit C, Schmidt-Ott KM, Schmidt-Ullrich R, and Muller DN. Tubular epithelial NF-kappaB activity regulates ischemic AKI. *J Am Soc Nephrol* 27: 2658–2669, 2016.
25. Maruyama T, Kanaji T, Nakade S, Kanno T, and Mikoshiba K. 2APB, 2-aminoethoxydiphenyl borate, a membrane-penetrable modulator of Ins(1,4,5)P3-induced Ca2+ release. *J Biochem* 122: 498–505, 1997.
26. Meng Y, Li T, Zhou GS, Chen Y, Yu CH, Pang MX, Li W, Li Y, Zhang WY, and Li X. The angiotensin-converting enzyme 2/angiotensin (1–7)/Mas axis protects against lung fibroblast migration and lung fibrosis by inhibiting the NOX4-derived ROS-mediated RhoA/Rho kinase pathway. *Antioxid redox signal* 22: 241–258, 2015.
27. Moennikes O, Buchmann A, Ott T, Willecke K, and Schwarz M. The effect of connexin32 null mutation on hepatocarcinogenesis in different mouse strains. Carcinogenesis 20: 1379–1382, 1999.
28. Narayanan A, Amaya M, Voss K, Chung M, Benedict A, Sampey G, Kehn-Hall K, Luchini A, Liotta L, Bailey C, Kumar A, Bavari S, Hakami RM, and Kashanchi F. Reactive oxygen species activate NFkappaB (p65) and p53 and induce apoptosis in RVFV infected liver cells. *Virology* 449: 270–286, 2014.
29. Park MH, Shim HS, Kim WH, Kim HJ, Kim DJ, Lee SH, Kim CS, Gwak MS, and Kim GS. Clinical risk scoring models for prediction of acute kidney injury after living donor liver transplantation: a retrospective observational study. *PLoS One* 10: e0136230, 2015.
30. Patel SJ, Milwid JM, King KR, Bohr S, Iracheta-Vellve A, Li M, Vitalo A, Parekkadan B, Jindal R, and Yarmush ML. Gap junction inhibition prevents drug-induced liver toxicity and fulminant hepatic failure. *Nat Biotechnol* 30: 179–183, 2012.
31. Peng J, Li X, Zhang D, Chen JK, Su Y, Smith SB, and Dong Z. Hyperglycemia, p53, and mitochondrial pathway of apoptosis are involved in the susceptibility of diabetic models to ischemic acute kidney injury. *Kidney Int* 87: 137–150, 2015.
32. Perico N, Cattaneo D, Sayegh MH, and Remuzzi G. Delayed graft function in kidney transplantation. *Lancet* 364: 1814–1827, 2004.
33. Piccoli C, D'Aprile A, Scrima R, Ambrosi L, Zefferino R, and Capitanio N. Subcytotoxic mercury chloride inhibits gap junction intercellular communication by a redox- and phosphorylation-mediated mechanism. *Free Radic Biol Med* 52: 916–927, 2012.
34. Picconi JL, Muff-Luett MA, Wu D, Bunchman E, Schaefer F, and Brophy PD. Kidney-specific expression of GFP by in-utero delivery of pseudotyped adeno-associated virus 9. *Mol Ther Methods Clin Dev* 1: 14014, 2014.
35. Rash JE, Yasumura T, Davidson KG, Furman CS, Dudek FE, and Nagy JI. Identification of cells expressing Cx43, Cx30, Cx26, Cx32 and Cx36 in gap junctions of rat brain and spinal cord. *Cell Commun Adhes* 8: 315–320, 2001.
36. Romanov V, Whyard TC, Waltzer WC, Grollman AP, and Rosenquist T. Aristolochic acid-induced apoptosis and G2 cell cycle arrest depends on ROS generation and MAP kinases activation. *Arch Toxicol* 89: 47–56, 2015.
37. Salvadori M, Rosso G, and Bertoni E. Update on ischemia-reperfusion injury in kidney transplantation: pathogenesis and treatment. *World J Transplant* 5: 52–67, 2015.
38. Senturk H, Kabay S, Bayramoglu G, Ozden H, Yaylak F, Yucel M, Olgun EG, and Kutlu A. Silymarin attenuates the renal ischemia/reperfusion injury-induced morphological changes in the rat kidney. *World J Urol* 26: 401–407, 2008.
39. Shimizu H, Saito S, Higashiyama Y, Nishijima F, Niwa T, and CREB. NF-kappaB, and NADPH oxidase coordinately upregulate indoxyl sulfate-induced angiotensinogen expression in proximal tubular cells. *Am J Physiol Cell Physiol* 304: C685–C692, 2013.
40. Sun LN, Liu XC, Chen XJ, Guan GJ, and Liu G. Curcumin attenuates high glucose-induced podocyte apoptosis by regulating functional connections between caveolin-1 phosphorylation and ROS. *Acta Pharmacol Sin* 37: 645–655, 2016.
41. Thirukkumaran C, Shi ZQ, Thirukkumaran P, Luider J, Kopciuk K, Spurrell J, Elzinga K, and Morris D. PUMA and NF-kB are cell signaling predictors of reovirus oncolysis of breast cancer. *PLoS One* 12: e0168233, 2017.
42. Udawatte C and Ripps H. The spread of apoptosis through gap-junctional channels in BHK cells transfected with Cx32. *Apoptosis Int J Programmed Cell Death* 10: 1019–1029, 2005.
43. Waggett AD, Benjamin M, and Ralphs JR. Connexin 32 and 43 gap junctions differentially modulate tenocyte response to cyclic mechanical load. *Eur J Cell Biol* 85: 1145–1154, 2006.
44. Wang P, Qiu W, Dudgeon C, Liu H, Huang C, Zambetti GP, Yu J, and Zhang L. PUMA is directly activated by NF-kappaB and contributes to TNF-alpha-induced apoptosis. *Cell Death Differ* 16: 1192–1202, 2009.
45. Wang YF, Shyu HW, Chang YC, Tseng WC, Huang YL, Lin KH, Chou MC, Liu HL, and Chen CY. Nickel (II)-induced cytotoxicity and apoptosis in human proximal tubule cells through a ROS- and mitochondria-mediated pathway. *Toxicol Appl Pharmacol* 259: 177–186, 2012.
46. Wong ET and Tergaonkar V. Roles of NF-kappaB in health and disease: mechanisms and therapeutic potential. *Clin Sci* 116: 451–465, 2009.
47. Wu SY, Leu YL, Chang YL, Wu TS, Kuo PC, Liao YR, Teng CM, and Pan SL. Physalin F induces cell apoptosis in human renal carcinoma cells by targeting NF-kappaB and generating reactive oxygen species. *PLoS One* 7: e40727, 2012.
48. Wu SY, Pan SL, Xiao ZY, Hsu JL, Chen MC, Lee KH, and Teng CM. NPRL-Z-1, as a new topoisomerase II poison, induces cell apoptosis and ROS generation in human renal carcinoma cells. *PLoS One* 9: e112220, 2014.
49. Xia N, Yan RY, Liu Q, Liao XH, Sun H, Guo H, and Zhang L. Augmenter of liver regeneration plays a protective role against hydrogen peroxide-induced oxidative stress in renal proximal tubule cells. *Apoptosis Int J Programmed Cell Death* 20: 423–432, 2015.
50. Xin Y, Li G, Liu H and D. Ai. AS-IV protects against kidney IRI through inhibition of NF-kappaB activity and PUMA upregulation. *Int J Clin Exp Med* 8: 18293–18301, 2015.
51. Xue JL, Daniels F, Star RA, Kimmel PL, Eggers PW, Molitoris BA, Himmelfarb J, and Collins AJ. Incidence and mortality of acute renal failure in Medicare beneficiaries, 1992 to 2001. *J Am Soc Nephrol* 17: 1135–1142, 2006.
52. Yang S, Zhu Z, Zhang X, Zhang N, and Yao Z. Idelalisib induces PUMA-dependent apoptosis in colon cancer cells. *Oncotarget* 8: 6102–6113, 2017.
53. Ye J, Li J, Xia R, Zhou M, and Yu L. Prohibitin protects proximal tubule epithelial cells against oxidative injury through mitochondrial pathways. *Free Radic Res* 49: 1393–1403, 2015.

54. Zhang L, Li YM, Jing YH, Wang SY, Song YF, and Yin J. Protective effects of carbenoxolone are associated with attenuation of oxidative stress in ischemic brain injury. *Neurosci Bull* 29: 311–320, 2013.

Address correspondence to:
Prof. Ziqing Hei
Department of Anesthesiology
The Third Affiliated Hospital of Sun Yat-sen University
No. 600 Tianhe Road
Guangzhou 510630
Guangdong Province
China

E-mail: heiziqing@sina.com

Prof. Dongdong Yuan
Department of Anesthesiology
The Third Affiliated Hospital of Sun Yat-sen University
No. 600 Tianhe Road
Guangzhou 510630
Guangdong Province
China

E-mail: yuandongdong123@126.com

Date of first submission to ARS Central, October 21, 2017; date of final revised submission, April 30, 2018; date of acceptance, May 22, 2018.

Abbreviations used

2-APB = 2-aminoethoxydiphenyl borate
AKI = acute kidney injury
Apaf-1 = apoptotic protease activating factor-1
BUN = blood urea nitrogen
Cr = creatinine
Cx = connexin
Cx32 = connexin 32
$Cx32^{-/-}$ = Cx32-gene knockdown
$Cx32^{+/+}$ = wild-type
Cx32-rAAV = Cx32-gene overexpression
DAPI = 6-diamino-2-phenylindole
DCFH-DA = 6-carboxy-2'-7'-dichlorodihydrofluorescein diacetate
DHE = dihydroethidium
DMEM = Dulbecco's Modified Eagle's medium
DPI = diphenyleneiodonium chloride
DRP1 = dynamin-related protein 1
FBS = fetal bovine serum
GJ = gap junction
H&E = hematoxylin–eosin staining
H24R4 = hypoxia for 24 h and reoxygenation for 4 h
HK-2 = human kidney tubular epithelial cell
HR = hypoxia reoxygenation
IF = immunofluorescence
IR = ischemia reperfusion
LDH = lactate dehydrogenase
MMP = mitochondrial membrane potential
MNF1 = mitochondrial nucleoid factor 1
NAC = N-acetyl cysteine
NRK52E = rat kidney tubular epithelial cell
PBS = phosphate-buffered saline
PFT-α = pifithrin-α
p-p65 = phosphorylated p65 nuclear factor-κB
PUMA = p53 upregulated modulator of apoptosis
qPCR = quantitative real-time polymerase chain reaction
rAAV = recombinant adeno-associated virus
ROS = reactive oxygen species
TUNEL = terminal deoxynucleotidyl transferase d UTP nick-end labeling